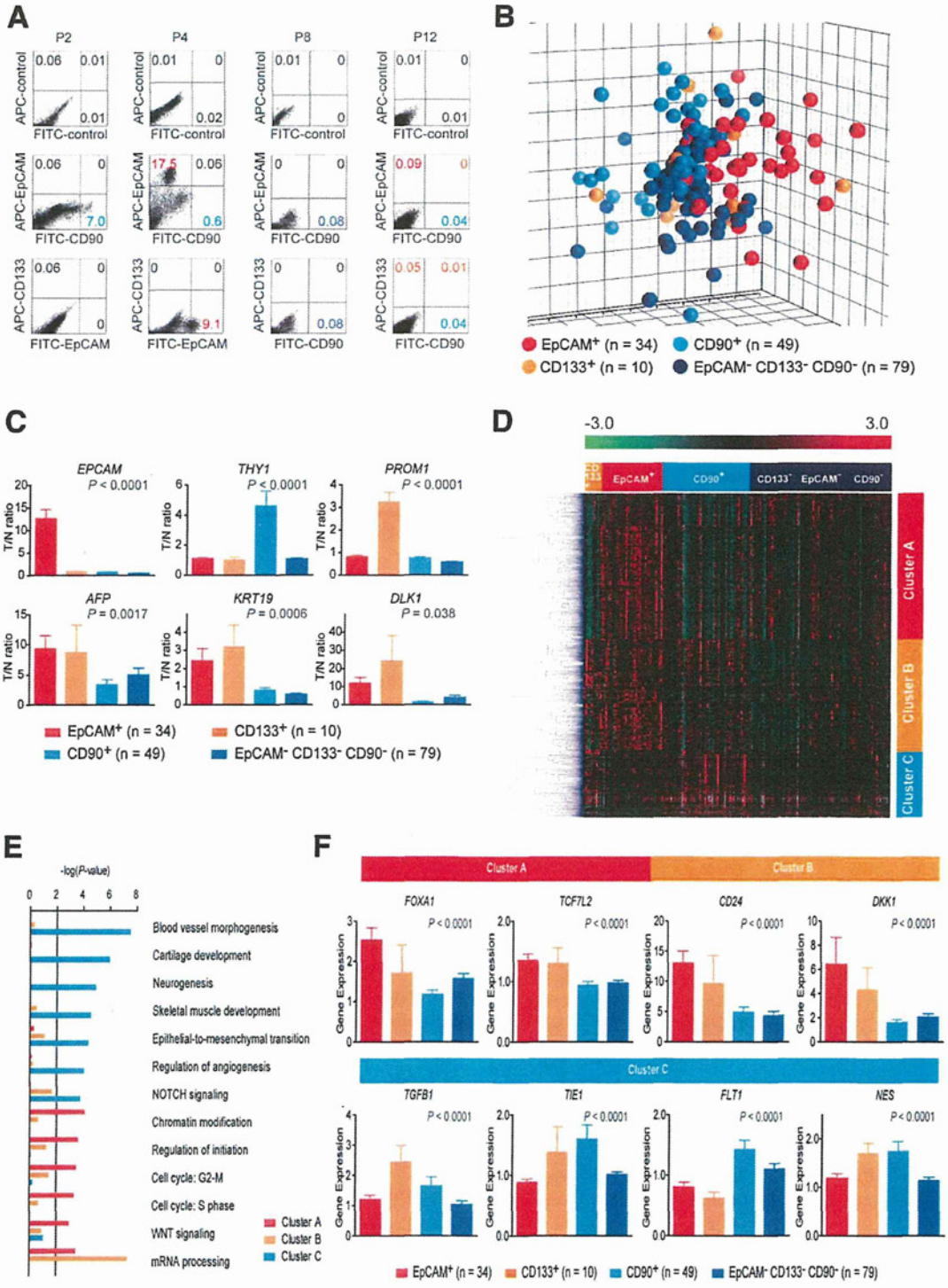

Fig. 1. Gene-expression profiles of CSC marker-positive HCCs. (A) FACS analysis of primary HCCs stained with fluorescent-labeled Abs against EpCAM, CD90, or CD133. (B) Multidimensional scaling analysis of 172 HCC cases characterized by the expression patterns of EpCAM, CD133, and CD90. Red, $EpCAM^+$ $CD90^-$ $CD133^-$ (n = 34); orange, $EpCAM^-$ $CD90^-$ $CD133^+$ (n = 10); light blue, $EpCAM^-$ $CD90^+$ $CD133^-$ (n = 49); blue, $EpCAM^-$ $CD90^-$ $CD133^-$ (n = 79). HCC specimens were clustered in specific groups with statistical significance ($P < 0.001$). (C) Expression patterns of well-known hepatic stem/progenitor markers in each HCC subtype, as analyzed by microarray. Red bar, $EpCAM^+$; orange bar, $CD133^+$; light blue bar, $CD90^+$; blue bar, $EpCAM^-$ $CD90^-$ $CD133^-$. (D) Hierarchical cluster analysis based on 1,561 EpCAM/CD90/CD133-coregulated genes in 172 HCC cases. Each cell in the matrix represents the expression level of a gene in an individual sample. Red and green cells depict high and low expression levels, respectively, as indicated by the scale bar. (E) Pathway analysis of EpCAM/CD90/CD133-coregulated genes. Canonical signaling pathways activated in cluster A (red bar), cluster B (orange bar), or cluster C (light blue bar) with statistical significance ($P < 0.01$) are shown. (F) Expression patterns of representative genes differentially expressed in EpCAM/CD90/CD133 HCC subtypes. Red bar, $EpCAM^+$; orange bar, $CD133^+$; light blue bar, $CD90^+$; blue bar, $EpCAM^-$ $CD133^-$ $CD90^-$.

Table 2. Tumorigenic Capacity of Unsorted, EpCAM$^+$, EpCAM$^-$, CD90$^+$, and CD90$^-$ Cells From Primary HCCs and Xenografts

Sample	CD133 (%)	CD90 (%)	EpCAM (%)	Cell Surface Marker	Number of Cells	Tumor Formation 2M	Tumor Formation 3M
P1	0	3.1	0	Unsorted	1×10^7	0/5	0/5
				CD90$^+$	1×10^5	0/5	0/5
				CD90$^-$	1×10^5	0/5	0/5
P2	0.06	7.0	0.06	Unsorted	1×10^7	0/5	0/5
				CD90$^+$	1×10^5	0/5	0/5
				CD90$^-$	1×10^5	0/5	0/5
P3	0	1.3	0	Unsorted	1×10^6	0/2	0/2
				CD90$^+$	1×10^4	0/4	0/4
				CD90$^-$	1×10^4	0/4	0/4
P4	0	0.6	17.5	Unsorted	1×10^6	3/4	4/4
				EpCAM$^+$	1×10^3	0/3	2/3
					1×10^4	3/4	4/4
					1×10^5	3/3	3/3
				CD90$^+$	1×10^3	0/3	0/3
					1×10^4	0/4	0/4
					1×10^5	0/3	0/3
				EpCAM$^-$ CD90$^-$	1×10^3	0/3	0/3
					1×10^4	0/4	0/4
					1×10^5	0/3	0/3
P5	0	0.8	29.7	Unsorted	1×10^6	0/5	0/5
				EpCAM$^+$	1×10^5	0/5	0/5
				CD90$^+$	1×10^5	0/5	0/5
				EpCAM$^-$ CD90$^-$	1×10^5	0/5	0/5
P6	0	0.7	0	Unsorted	1×10^6	0/2	0/2
				CD90$^+$	1×10^4	0/4	0/4
				CD90$^-$	1×10^4	0/4	0/4
P7	1.38	4.5	4.4	Unsorted	1×10^6	2/2	2/2
				EpCAM$^+$	2×10^2	0/3	0/3
					1×10^3	0/3	1/3
					1×10^4	2/4	4/4
				CD90$^+$	2×10^2	0/3	0/3
					1×10^3	0/3	0/3
					1×10^4	0/4	0/4
				EpCAM$^-$ CD90$^-$	1×10^3	0/3	0/3
					1×10^4	0/3	0/3
					1×10^5	0/4	0/4
P8	0	0.08	0	Unsorted	1×10^5	0/4	0/4
				CD90$^+$	1×10^3	0/3	0/3
				CD90$^-$	1×10^5	0/3	0/3
P9	0	0.26	0	Unsorted	1×10^5	0/4	0/4
				CD90$^+$	1×10^3	0/3	0/3
				CD90$^-$	1×10^5	0/3	0/3
P10	0	0.78	0	Unsorted	1×10^4	0/4	0/4
				CD90$^+$	1×10^3	0/3	0/3
				CD90$^-$	1×10^4	0/3	0/3
P11	0	0.1	1.54	Unsorted	5×10^4	0/2	0/2
				EpCAM$^+$	1×10^3	0/3	0/3
				CD90$^+$	1×10^3	0/3	0/3
				EpCAM$^-$ CD90$^-$	1×10^4	0/3	0/3
P12	0.06	0.05	0.09	Unsorted	1×10^5	0/3	3/3
				CD90$^+$	1×10^3	0/4	1/4
				CD90$^-$	1×10^3	0/4	1/4
					1×10^4	0/3	3/3
P13	0	0.03	67.7	EpCAM$^+$	5×10^5	4/4	NA
					5×10^4	3/3	NA
					5×10^3	3/3	NA
				EpCAM$^-$	5×10^5	0/4	NA
					5×10^4	0/3	NA
					5×10^3	0/3	NA
P14	24.0	0.06	3.1	EpCAM$^+$	5×10^3	4/5	NA
				EpCAM$^-$	5×10^3	2/5	NA
P15	0	2.45	0	CD90$^+$	5×10^4	3/4	NA
					5×10^3	1/3	NA
					5×10^2	1/3	NA
				CD90$^-$	5×10^4	2/4	NA
					5×10^3	1/3	NA
					5×10^2	0/3	NA

NA, not available.

contained definite CD133$^+$ cells (20%) (Table 2). CD90$^+$ cells were detected at variable frequencies in all 15 HCCs analyzed.

To explore the status of these CSC marker-positive cells in HCC in a large cohort, we utilized oligo-DNA microarray data from 238 HCC cases (GEO accession no.: GSE5975) to evaluate the expression of *EPCAM* (encoding EpCAM and CD326), *THY1* (encoding CD90), and *PROM1* (encoding CD133) in whole HCC tissues and nontumor (NT) tissues. Because previous studies demonstrated that CD133$^+$ and CD90$^+$ cells were detected at low frequency (~13.6% by CD133 staining and ~6.2% by CD90 staining) in HCC, but were almost nonexistent in NT liver (4, 5),[4,5] we utilized tumor/nontumor (T/N) gene-expression ratios to detect the existence of marker-positive CSCs in tumor. Accordingly, we showed that a 2-fold cutoff of T/N ratios of *EPCAM* successfully stratifies HCC samples with EpCAM$^+$ liver CSCs.[9,10]

A total of 95 (39.9%), 110 (46.2%), and 31 (13.0%) of the 238 HCC cases were thus regarded as EpCAM$^+$, CD90$^+$, and CD133$^+$ HCCs (T/N ratios: $\geq$2.0), respectively. As observed in the FACS data described above, we detected coexpression of EpCAM and CD90 in 45 HCCs (18.9%), EpCAM and CD133 in five HCCs (2%), CD90 and CD133 in five HCCs (2%), and EpCAM, CD90, and CD133 in 11 HCCs (4.6%). To clarify the characteristics of gene-expression signatures specific to stem cell marker expression status, we selected 172 HCC cases expressing a single CSC marker (34 EpCAM$^+$ CD90$^-$ CD133$^-$, 49 EpCAM$^-$ CD90$^+$ CD133$^-$, and 10 EpCAM$^-$ CD90$^-$ CD133$^+$) or all marker-negative HCCs (79 EpCAM$^-$ CD90$^-$ CD133$^-$). A class-comparison analysis with

univariate F tests and a global permutation test (×10,000) yielded a total of 1,561 differentially expressed genes. Multidimensional scaling (MDS) analysis using this gene set indicated that HCC specimens were clustered in specific groups with statistical significance ($P < 0.001$). Close examination of MDS plots revealed three major HCC subtype clusters: all marker-negative HCCs (blue spheres); EpCAM single-positive HCCs (red spheres); and CD90 single-positive HCCs (light blue spheres). $CD133^+$ HCCs (orange spheres) were rare, relatively scattered, and not clustered (Fig. 1B).

We examined the expression of representative hepatic stem/progenitor cell markers *AFP*, *KRT19*, and *DLK1* in HCCs with regard to the gene-expression status of each CSC marker (Fig. 1C). All three markers were up-regulated in $EpCAM^+$ and $CD133^+$ HCCs, compared with all marker-negative HCCs, consistent with previous findings.[10,11] However, we found no significant overexpression of *AFP*, *KRT19*, and *DLK1* in $CD90^+$ and all marker-negative HCCs.

Hierarchical cluster analyses revealed three main gene clusters that were up-regulated in $EpCAM^+$ HCCs (cluster A, 706 genes), $EpCAM^+$ or $CD133^+$ HCCs (cluster B, 530 genes), and $CD90^+$ or $CD133^+$ HCCs (cluster C, 325 genes) (Fig. 1D). Pathway analysis indicated that the enriched genes in cluster A (red bar) were associated with chromatin modification, cell-cycle regulation, and Wnt/β-catenin signaling (Fig. 1E). Genes associated with messenger RNA processing were enriched in clusters A (red bar) and B (orange bar). Surprisingly, genes in cluster C were significantly associated with pathways involved in blood-vessel morphogenesis, angiogenesis, neurogenesis, and epithelial mesenchymal transition (EMT) (light blue bar). Close examination of genes in each cluster suggested that known hepatic transcription factors (*FOXA1*), Wnt regulators (*TCF7L2* and *DKK1*), and a hepatic stem cell marker (*CD24*) were dominantly up-regulated in $EpCAM^+$ and $CD133^+$ HCCs (Fig. 1F). By contrast, genes associated with blood-vessel morphogenesis (*TIE1* and *FLT1*), EMT (*TGFB1*), and neurogenesis (*NES*) were activated dominantly in $CD90^+$ HCCs and $CD133^+$ HCCs.

$CD90^+$ HCC Cells Share Features With Mesenchymal Vascular Endothelial Cells. Because $CD133^+$ HCCs were relatively rare and constituted only 13% (microarray cohort) to 20% (FACS cohort) of all HCC samples analyzed, we focused on the characterization of EpCAM and CD90. To clarify the cell identity of $EpCAM^+$ or $CD90^+$ cells in primary HCCs, we performed IHC analysis of 18 needle-biopsy specimens of premalignant dysplastic nodules (DNs), 102 surgically resected HCCs, and corresponding NT liver tissues. When examining the expression of EpCAM and CD90 in cirrhotic liver tissue by double-color IHC analysis, we found that $EpCAM^+$ cells and $CD90^+$ cells were distinctively located and not colocalized (Supporting Fig. 1A). Immunoreactivity (IR) to anti-CD90 antibodies (Abs) was detected in vascular endothelial cells (VECs), inflammatory cells, fibroblasts, and neurons, but not in hepatocytes or cholangiocytes, in the cirrhotic liver (Supporting Fig. 1B, panels a,b). IR to anti-EpCAM Abs was detected in hepatic progenitors adjacent to the periportal area and bile duct epithelial cells in liver cirrhosis (Supporting Fig. 1B, panels c,d).

IR to anti-EpCAM Abs was detected in 37 of 102 surgically resected HCCs (Fig. 2A, panel b), but not in 18 DNs (Fig. 2A, panel a). By contrast, no tumor epithelial cells (TECs) showing IR to anti-CD90 Abs were found in any of the 18 DNs or 102 HCCs examined (Fig. 2A, panels c,d). However, we identified $CD90^+$ cells that were morphologically similar to VECs or fibroblasts within the tumor nodule in 37 of the 102 surgically resected HCC tissues (≥5% positive staining in a given area). IR to anti-CD90 Abs was also detected in hepatic mesenchymal tumors (Supporting Fig. 1C, panels a-c), indicating that CD90 is also a marker of liver stromal tumors.

Double-color IHC and immunofluorescence (IF) analysis confirmed the distinct expression of EpCAM and CD90 in HCC (Fig. 2B), consistent with the FACS data (Fig. 1A). Quantitative real-time polymerase chain reaction (qPCR) analysis of sorted $EpCAM^+$, $CD90^+$, and $EpCAM^-$ $CD90^-$ cells after $CD45^+$ cell depletion indicated that the hepatic stem/progenitor markers, *AFP* and *KRT19*, were up-regulated in $EpCAM^+$ cells (red bar), whereas the mesenchymal markers, *KIT* and *FLT1*, were up-regulated in $CD90^+$ cells (orange bar), compared with $EpCAM^-$ $CD90^-$ cells (blue bar) (Fig. 2C). The hepatocyte marker, *CYP3A4*, was down-regulated in $EpCAM^+$ cells and not detected in $CD90^+$ cells, compared with $EpCAM^-$ $CD90^-$ cells. *POU5F1* and *BMI1* were equally up-regulated in both $EpCAM^+$ and $CD90^+$ cells, compared with $EpCAM^-$ $CD90^-$ cells.

EpCAM and CD90 were independently and distinctively expressed in different cellular lineages, so we evaluated the staining of EpCAM and CD90 separately and analyzed the clinicopathological characteristics of surgically resected HCC cases. HCCs were regarded marker positive if ≥5% positive staining was detected in a given area. The existence of $EpCAM^+$

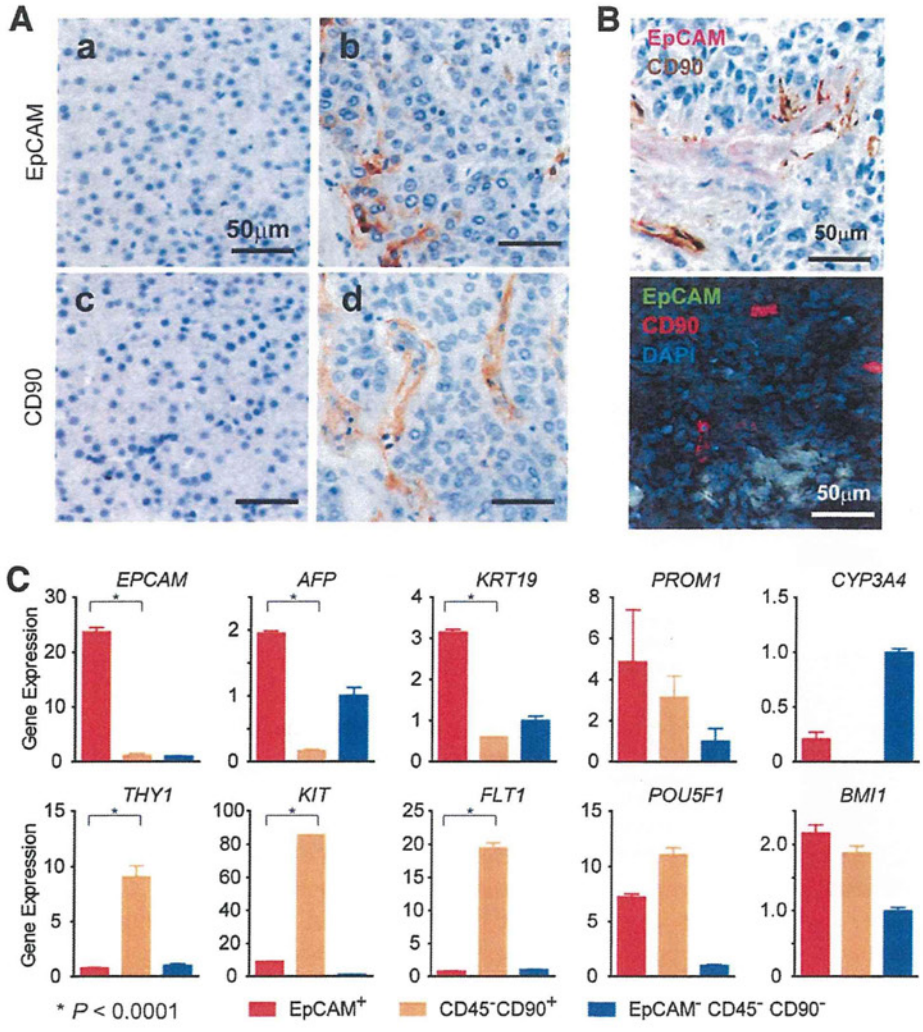

Fig. 2. Distinct EpCAM$^+$ and CD90$^+$ cell populations in HCC. (A) Representative images of EpCAM and CD90 staining in dysplastic nodule (panels a,c) and HCC (panels b,d) by IHC analysis (scale bar, 50 μm). EpCAM (panels a,b) and CD90 (panels c,d) immunostaining is depicted. (B) Upper panel: representative images of EpCAM (red) and CD90 (brown) double staining in HCC by IHC (scale bar, 50 μm). Lower panel: representative images of EpCAM (green) and CD90 (red) staining with 4'6-diamidino-phenylindole (DAPI) (blue) in HCC by IF (scale bar, 50 μm). (C) qPCR analysis of sorted EpCAM$^+$ (red bar), CD90$^+$ (orange bar), or EpCAM$^-$ CD90$^-$ (blue bar) derived from a representative primary HCC. Experiments were performed in triplicate, and data are shown as mean ± standard error of the mean.

cells (≥5%) was characterized by poorly differentiated morphology and high serum AFP values with a tendency for portal vein invasion, whereas the existence of CD90$^+$ cells (≥5%) was associated with poorly differentiated morphology and a tendency for large tumor size (Supporting Tables 2 and 3). Notably, the existence of CD90$^+$ cells was associated with a high incidence of distant organ metastasis, including lung, bone, and adrenal gland, within 2 years after surgery, whereas EpCAM$^+$ cell abundance appeared unrelated to distant organ metastasis.

We evaluated the characteristics of EpCAM$^+$ or CD90$^+$ cells in seven representative HCC cell lines. Morphologically, all EpCAM$^+$ cell lines (HuH1, HuH7, and Hep3B) showed a polygonal, epithelial cell shape, whereas three of four CD90$^+$ cell lines (HLE, HLF, and SK-Hep-1) showed a spindle cell shape (Fig. 3A). EpCAM$^+$ cells were detected in 11.5%, 57.7%, and 99.6% of sorted HuH1, HuH7, and Hep3B cells, respectively. A small CD90$^+$ cell population (0.66%) was observed in PLC/PRL/5, whereas 91.3%, 10.8%, and 59.0% of CD90$^+$ cells were detected in HLE, HLF, and SK-Hep-1, respectively. Compared with primary HCCs, only EpCAM$^+$ or CD90$^+$ cells were detected in liver cancer cell lines under normal culture conditions (Fig. 3B), suggesting that these cell lines contain a relatively pure cell population most likely obtained by clonal selection through the establishment process.

A class-comparison analysis with univariate t tests and a global permutation test (×10,000) of microarray data yielded two main gene clusters up-regulated in EpCAM$^+$ cell lines (HuH1, HuH7, and Hep3B) (cluster I, 524 genes) or in CD90$^+$ cell lines (HLE, HLF, and SK-Hep-1) (cluster II, 366 genes) (Fig. 3C). PLC/PRL/5 showed intermediate gene-expression patterns between EpCAM$^+$ and CD90$^+$ cell lines using this gene set. Pathway analysis indicated that the genes

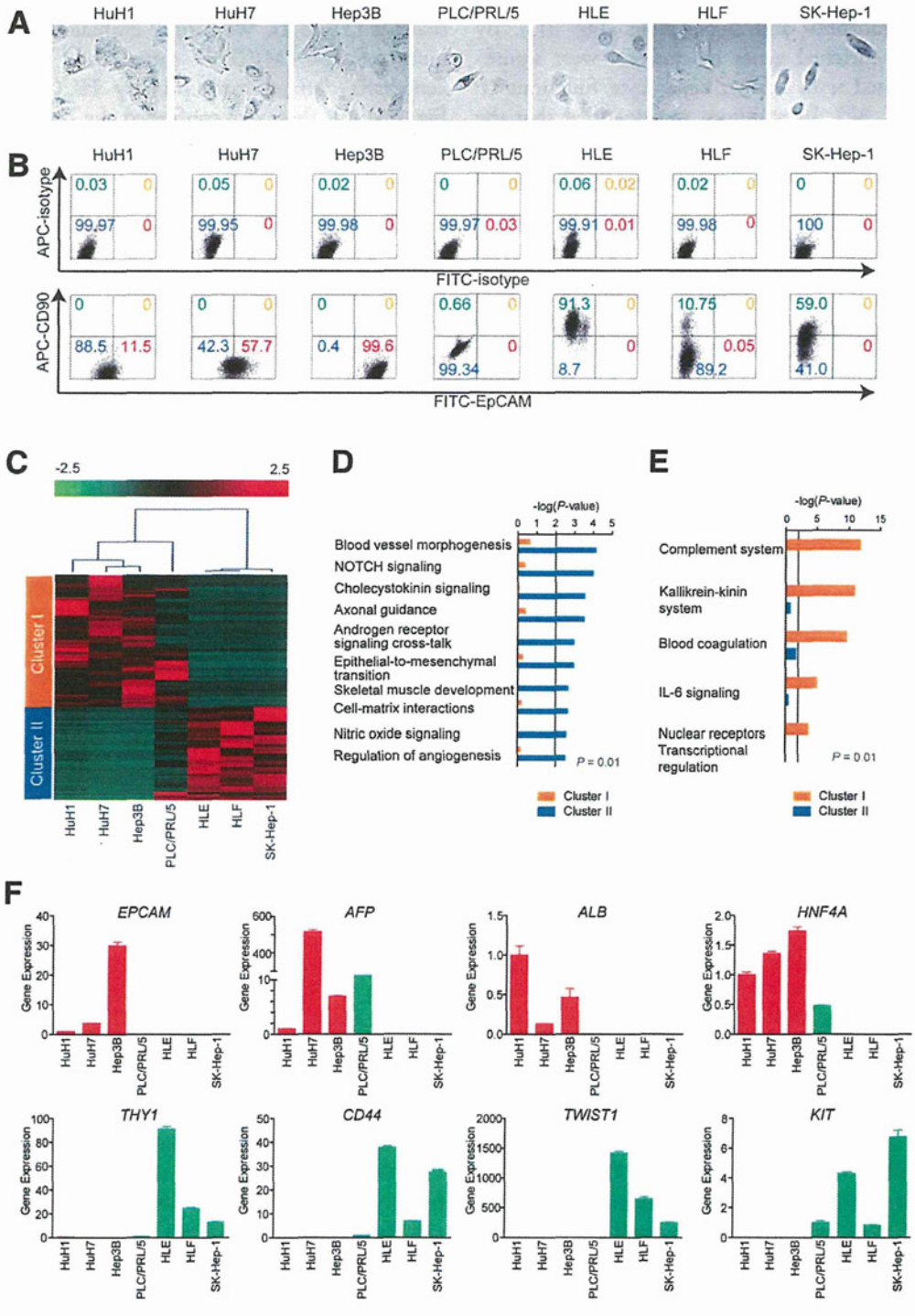

Fig. 3. Characteristics of HCC cell lines defined by EpCAM and CD90. (A) Representative photomicrographs of EpCAM^{+}CD90^{-} and EpCAM^{-} CD90^{+} HCC cell lines. (B) Representative FACS data of EpCAM^{+}CD90^{-} and EpCAM^{-} CD90^{+} HCC cell lines stained with fluorescein isothiocyanate (FITC)-EpCAM and APC-CD90 Abs. (C) Heat-map images of seven HCC cell lines based on 890 EpCAM/CD90-coregulated genes. Each cell in the matrix represents the expression level of a gene in an individual sample. Red and green cells depict high and low expression levels, respectively, as indicated by the scale bar. (D and E) Pathway analysis of EpCAM/CD90-coregulated genes. Canonical signaling pathways activated in cluster I (orange bar) or II (blue bar) with statistical significance ($P < 0.01$) are shown. (F) qPCR of representative differentially expressed genes identified by microarray analysis (C) in seven HCC cell lines.

enriched in cluster II were mainly associated with blood-vessel morpho- and angiogenesis (Fig. 3D). By contrast, the enriched genes in cluster I were significantly associated with known hepatocyte functions ($P < 0.01$) (Fig. 3E). In addition, we identified that the enriched genes in cluster II were significantly associated with neurogenesis, skeletal muscle development, and EMT.

We used qPCR to validate that known hepatic stem cell (HSC) and hepatocyte markers, such as *AFP, EPCAM, ALB*, and *HNF4A* genes, were up-regulated in $EpCAM^+$ cell lines, but not detected in $CD90^+$ cell lines (Fig. 3F). By contrast, genes associated with mesenchymal lineages and EMT, such as *KIT, TWIST1, CD44*, and *THY1*, were strongly up-regulated in $CD90^+$ cell lines.

Unique Tumorigenicity and Metastasis Capacity of Distinct CSCs Defined by EpCAM and CD90. We investigated the tumorigenic capacity of $EpCAM^+$ or $CD90^+$ cells by subcutaneously (SC) injecting 1×10^5 sorted cells of four HCC cell lines (HuH1, HuH7, HLE, and HLF) into nonobese diabetic, severe combined immunodeficient (NOD/SCID) mice. We excluded Hep3B cells for the evaluation of tumorigenicity because almost 100% of cells were EpCAM positive. We further excluded SK-Hep-1 cells from the analysis because they potentially originated from endothelial cells.[12] The highly tumorigenic capacities of $EpCAM^+$ and $CD90^+$ cells were reproduced in HuH1, HuH7, and HLF cell lines, compared with marker-negative cells (Fig. 4A). However, HLE cells did not produce SC tumors, even 12 months after transplantation, in NOD/SCID mice. $EpCAM^+$ cells from HuH1 and HuH7 formed larger tumors more rapidly than $CD90^+$ cells from HLF (Fig. 4B). IHC analyses indicated that $EpCAM^+$ cells did not produce $CD90^+$ cells and *vice versa* in these cell lines *in vivo* (Fig. 4C). $CD90^+$ cells showed a high metastatic capacity, whereas $EpCAM^+$ cells showed no metastasis to the lung when SC tumor volume reached approximately 2,000 (HuH1 and HuH7) or 700 mm^3 (HLF) (Fig. 4D). The high metastatic capacity of PLC/PRL/5 cells, which contain a small population of $CD90^+$ cells, was also confirmed after SC injection into NOD/SCID mice (data not shown). $CD90^+$ cells could divide to generate both $CD90^+$ and $CD90^-$ cells, and $CD90^+$ cells showed a high capacity to invade and form spheroids with overexpression of *TWIST1* and *TWIST2*, which are known to activate EMT programs in HLF cells (Supporting Fig. 2A-D).

We next evaluated the tumorigenic/metastatic capacity of $CD45^-$ tumor cells using 12 fresh primary HCC specimens (P1-P12) that had been surgically resected (Table 2). We further evaluated the tumorigenicity of EpCAM/CD90 sorted cells obtained from xenografts derived from primary HCCs (Supporting Fig. 3A). Of these, we confirmed the tumorigenicity of cancer cells obtained from six primary HCCs after SC injection into NOD/SCID mice within 3 months after transplantation (Fig. 5A; Table 2; Supporting Fig. 3B). $EpCAM^+$ cells derived from four HCCs (P4, P7, P13, and P14) showed highly tumorigenic capacities, compared with $EpCAM^-$ cells. $CD90^+$ cells derived from two HCCs showed equal (P12) or more-tumorigenic capacities (P15), compared with $CD90^-$ cells. Tumorigenicity of $EpCAM^+$ cells was observed in three hepatitis C virus (HCV)-related HCCs and an hepatitis B virus (HBV)-related HCC, whereas tumorigenicity of $CD90^+$ cells was observed in two HBV-related HCCs (Tables 1 and 2).

Using unsorted cells, we compared the frequency of $EpCAM^+$ and $CD90^+$ cells in primary and xenograft tumors and found that $EpCAM^+$ cells remained, but $CD90^+$ cells disappeared, in secondary tumors derived from P4 or P7, whereas $EpCAM^+$ cells disappeared, but $CD90^+$ cells remained, in secondary tumors derived from P12 (Fig. 5B). Morphologically, tumorigenic $EpCAM^+$ cells showed an epithelial cell shape, whereas $CD90^+$ cells showed a mesenchymal VEC shape (Fig. 5C and Supporting Fig. 3C). FACS analysis indicated that P12 HCC cells showed abundant expression of vascular endothelial growth factor receptor (VEGFR) 1 and a vascular endothelial marker endoglin (CD105) (Fig. 5D). By contrast, P4 and P7 HCC cells did not express these vascular endothelial markers (data not shown). Lung metastasis was detected in NOD/SCID mice transplanted with P12 HCC cells, but not in mice transplanted with P4 and P7 HCC cells (Fig. 5E,F).

Taken together, these results suggest that the tumorigenic and metastatic capability of primary HCC may depend on the presence of distinct $EpCAM^+$ or $CD90^+$ CSCs. $EpCAM^+$ cells were associated with a high tumorigenic capacity with hepatic epithelial stem cell features, whereas $CD90^+$ cells were related to the metastatic propensity with VEC features.

Suppression of Lung Metastasis Mediated by $CD90^+$ CSCs by Imatinib Mesylate. We previously demonstrated that Wnt/β-catenin signaling inhibitors could successfully attenuate the tumorigenic capacity of $EpCAM^+$ CSCs in HCC.[8,10] To explore the potential molecular targets activated in $CD90^+$ CSCs, we investigated the expression of the known VEC markers, CD105, VEGFR1 (encoded by *FLT1*), and

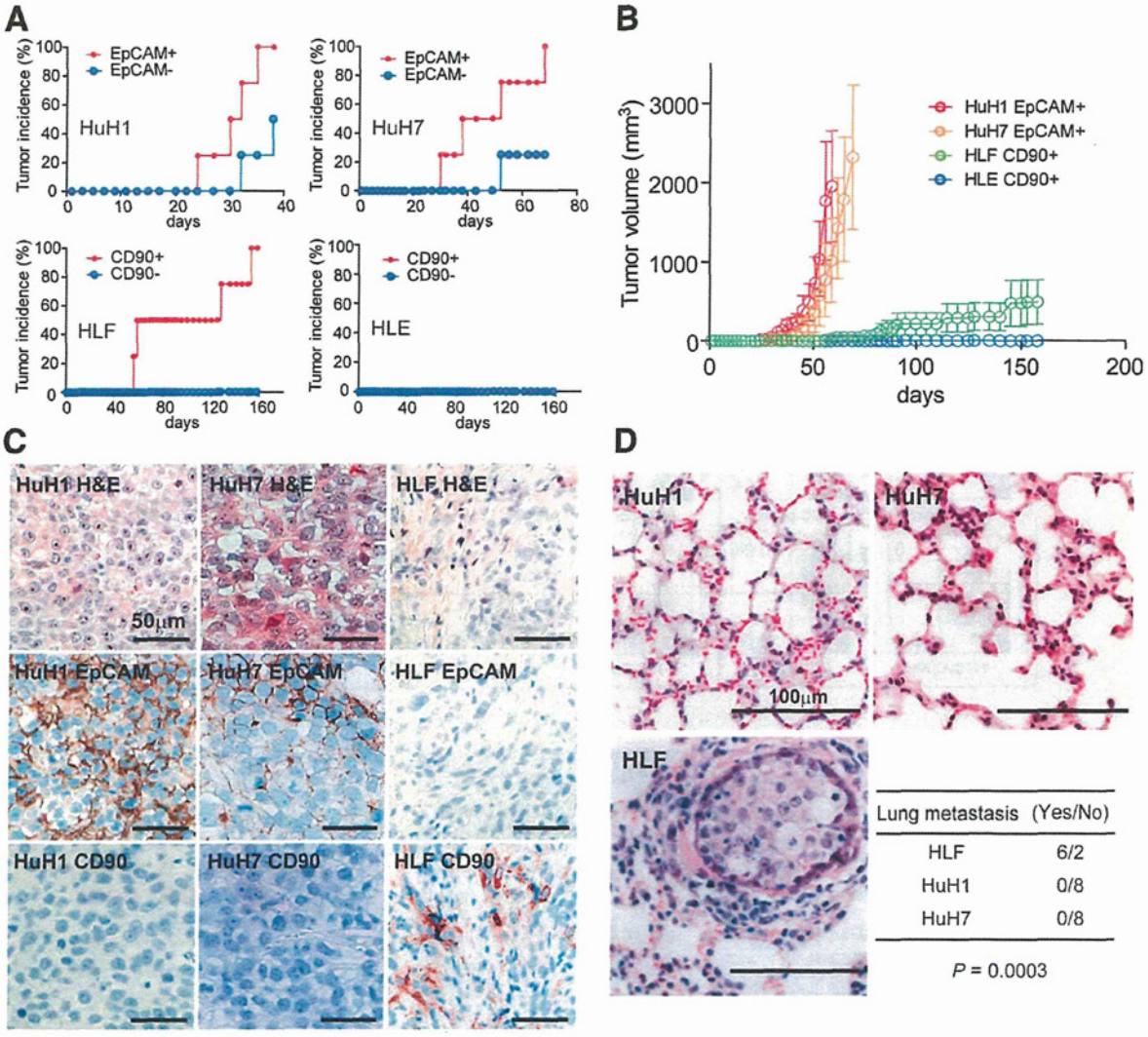

Fig. 4. Distinct tumorigenic/metastatic capacities of HCC cell lines defined by EpCAM and CD90. (A) Tumorigenicity of 1×10^5 cells sorted by anti-EpCAM (HuH1 and HuH7) or anti-CD90 (HLE and HLF) Abs. Data are generated from 8 mice/cell line. (B) Tumorigenic ability of $EpCAM^+$ and $CD90^+$ sorted cells in NOD/SCID mice. Aggressive tumor growth in the SC lesion was observed in $EpCAM^+$ HuH1 or HuH7 cells, compared with $CD90^+$ HLE or HLF cells. $EpCAM^+$ (1×10^5) or $CD90^+$ cells were injected. Tumor-volume curves are depicted as mean ± standard deviation of 4 mice/group. (C) Histological analysis of $EpCAM^+$ or $CD90^+$ cell-derived xenografts. Hematoxylin and eosin (H&E) staining of a SC tumor (upper panels) and IHC of the tumor with anti-EpCAM (middle panels) or anti-CD90 Abs (bottom panels) are shown (scale bar, 50 μm). (D) Metastasis was evaluated macroscopically and microscopically in the left and right lobes of the lung separately in each mouse (n = 4) (scale bar, 100 μm).

c-Kit (encoded by *KIT*), in cell lines and showed that they were abundantly expressed in $CD90^+$ cell lines, but not $EpCAM^+$ cell lines (Fig. 6A). No expression of VEGFR2 was detected in this set of cell lines, suggesting that molecular reagents specifically targeting VEGFR2 may have no effects on $CD90^+$ CSCs. CD44, a stem cell marker that functionally regulates redox status and is a potential target of $CD90^+$ CSCs, was also abundantly expressed in $CD90^+$ cell lines (Supporting Fig. 4A), consistent with previous data.[5,13] No significant difference was detected in the expression of the hematopoietic marker, CD34, or ABCG2 between $EpCAM^+$ and $CD90^+$ cell lines (Supporting Fig. 4A).

Among these molecular targets, we focused on the characterization of c-Kit because the c-Kit tyrosine kinase inhibitor, imatinib mesylate, is readily available, is widely used for the treatment of gastrointestinal stromal tumor with activation of c-Kit, and may have potential antitumor activity against a subset of HCC.[14] We explored the effect of imatinib mesylate on HCC cell lines and found that treatment with 10

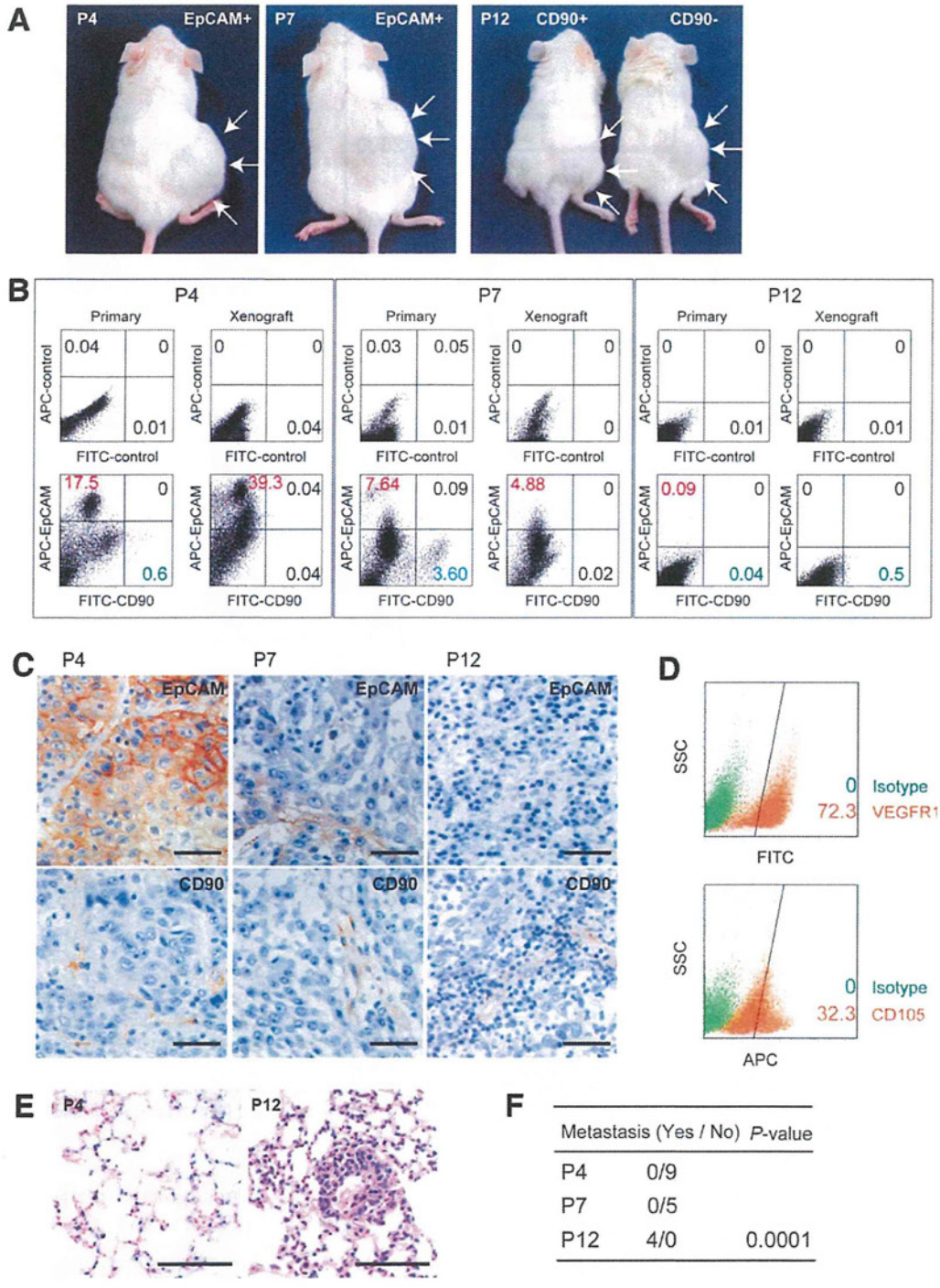

Fig. 5. Tumorigenic/metastatic capacities of EpCAM$^+$ and CD90$^+$ cells in primary HCC. (A) Representative NOD/SCID mice with SC tumors (white arrows) from EpCAM$^+$ P4 or P7 cells (left and middle panels) and CD90$^+$ or CD90$^-$ P12 cells (right panel). (B) FACS analysis of CD90 and EpCAM staining in primary HCCs and the corresponding secondary tumors developed in NOD/SCID mice. Unsorted cells (1×10^6 cells in P4 and P7 or 1×10^5 cells in P12) were SC injected to evaluate the frequency of each marker-positive cell in primary and secondary tumors. (C) IHC analysis of EpCAM and CD90 in primary HCCs P4, P7, and P12 (scale bar, 50 μm). (D) FACS analysis of VEGFR1 (Alexa488) and CD105 (APC) in primary HCC P12. (E) Hematoxylin and eosin staining of lung tissues in P4 and P12 (scale bar, 200 μm). (F) Frequency of lung metastasis in NOD/SCID mice SC transplanted using unsorted primary HCC cells.

μM reduced cell proliferation and spheroid formation in CD90$^+$ cell lines, but had no effect on EpCAM$^+$ cell lines (Supporting Fig. S4B,C).

We further explored the effect of imatinib mesylate *in vivo*. Because EpCAM$^+$ and CD90$^+$ cells reside in the primary HCC, but not in established cell lines, we SC injected HuH7 and HLF cell lines to generate tumors organized by EpCAM$^+$ and CD90$^+$ CSCs. Interestingly, when HLF cells were coinjected with HuH7 cells, EpCAM$^+$ cells could metastasize to the lung, whereas

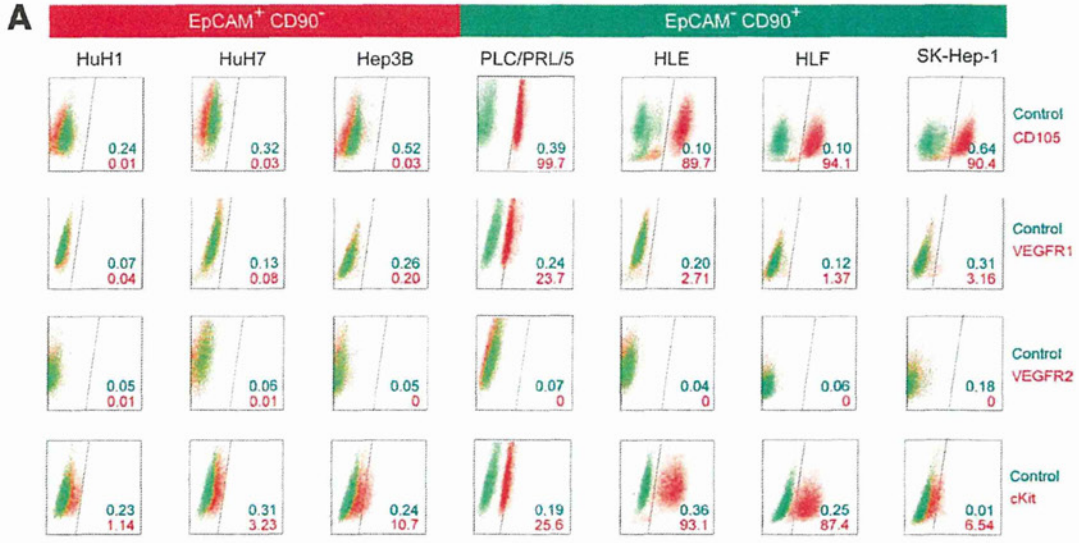

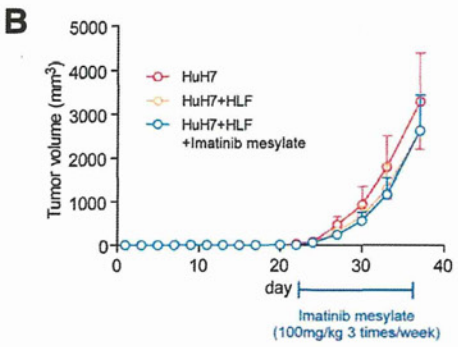

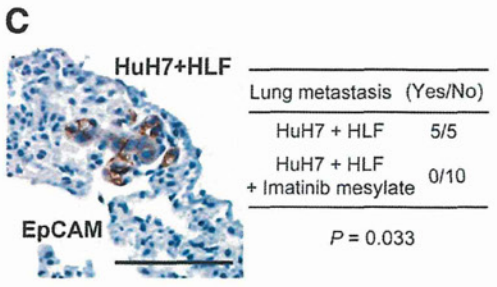

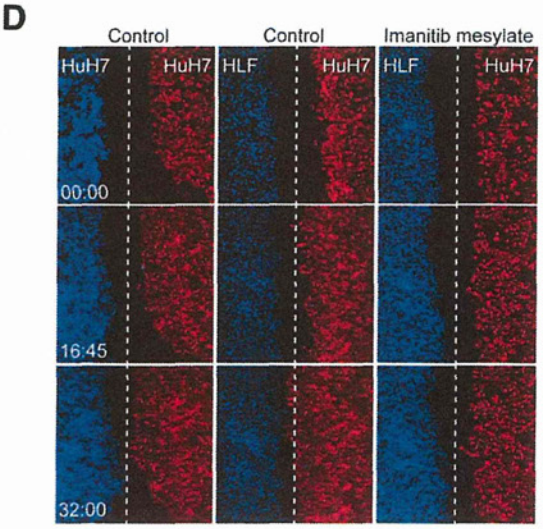

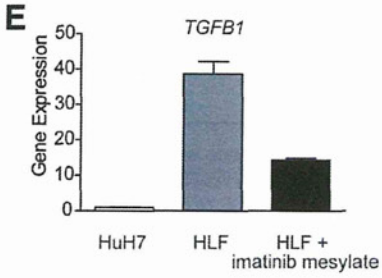

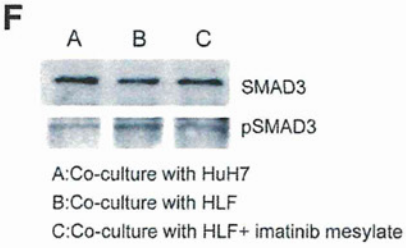

SC primary tumors showed no difference in size (Fig. 6B,C). Furthermore, although imatinib mesylate treatment had little effect on the size of primary SC tumors, it significantly suppressed lung metastasis in primary tumors (Fig. 6C). These data suggest that $CD90^+$ cells are not only metastatic to the distant organ, but also help the metastasis of $CD90^-$ cells, including $EpCAM^+$ cells, which originally have no distant metastatic capacity. Our data further suggest that imatinib mesylate can inhibit distant organ metastasis by suppressing $CD90^+$ metastatic CSCs, albeit with little effect on $EpCAM^+$ tumorigenic epithelial stem-like CSCs.

To explore the potential mechanism of how $CD90^+$ cells dictate the metastasis of $EpCAM^+$ cells, we utilized coculture systems and time-lapse image analysis. Wound-healing analysis clearly indicated that motility of HuH7 cells was enhanced when HLF cells were cocultured, and this effect was abolished by imatinib mesylate treatment (Fig. 6D; see Supporting Videos 1-3). HLF cells abundantly expressed *TGFB1*, compared with HuH7 cells, and its expression was dramatically suppressed by imatinib mesylate treatment (Fig. 6E). Mothers against decapentaplegic homolog 3 (Smad3) phosphorylation was augmented in HuH7 cells when cocultured with HLF cells, and this effect was attenuated when cocultured with HLF cells pretreated with imatinib mesylate.

Taken together, our data suggest that liver CSCs are not a single entity. Liver CSCs defined by different markers show unique features of tumorigenicity/metastasis with phenotypes closely associated with committed liver lineages. These distinct CSCs may collaborate to enhance tumorigenicity and metastasis of HCCs.

Discussion

The current investigation demonstrates that CSC marker expression status may be a key determinant of cancer phenotypes, in terms of metastatic propensity and chemosensitivity, to certain molecularly targeted therapies. EpCAM appears to be an epithelial tumorigenic CSC marker, whereas CD90 seems to be a mesenchymal metastatic CSC marker associated with expression of c-Kit and chemosensitivity to imatinib mesylate. Imatinib mesylate may be effective in inhibiting metastasis, but has little effect on primary $EpCAM^+$ HCC cell growth.

We investigated the frequency of three CSC markers (EpCAM, CD90, and CD133) in 15 primary HCCs with a confirmed cell viability of $\geq$70% and found that three HCCs contained $CD133^+$ cells, seven HCCs contained $EpCAM^+$ cells, and all HCCs contained $CD90^+$ cells. Among them, we confirmed the perpetuation of $CD133^+$ cells derived from three HCCs (P7, P12, and P14; data not shown), $EpCAM^+$ cells derived from four HCCs (P4, P7, P13, and P14), and $CD90^+$ cells derived from two HCCs (P12 and P15). Recent studies showed that at least 8 of 21 HCCs (38%)[4] and 13 of 13 HCCs (100%)[5] contained tumorigenic $CD133^+$ or $CD90^+$ CSCs, respectively. Recent IHC and tissue microarray studies also demonstrated that $CD133^+$ and $CD90^+$ cells were detected in 24.8% ($\geq$1% of tumor cells) and 32.2% ($\geq$5% of tumor cells) of HCC cases examined, respectively.[15,16]

One possible explanation of the comparatively low frequency of $CD133^+$ liver CSCs identified in our study is that we used the monoclonal Ab CD133/2, whereas Ma et al. used CD133/1. Another possible explanation is the difference of etiology related to hepatocarcinogenesis. We examined tumorigenicity using 15 HCCs (five HBV related, four HCV related, three non-B, non-C hepatitis [NBNC] related, and three alcohol related) and identified that tumorigenic CSCs were only obtained from HBV- or HCV-related cases. Previous liver CSC studies were performed using HBV-related HCCs,[4,5] and a recent study showed that

Fig. 6. Suppression of lung metastasis mediated by $CD90^+$ CSCs by imatinib mesylate. (A) FACS analysis of seven HCC cell lines stained by APC-CD105, Alexa 488/VEGFR1, APC/VEGFR2, and Alexa 488/c-Kit Abs or isotype control. (B) Tumorigenicity of 5×10^5 HuH7 cells and 2.5×10^5 HuH7 cells plus 2.5×10^5 HLF cells treated with imatinib mesylate or control phosphate-buffered saline (PBS) (200 μL/mouse) orally ingested three times per week (100 mg/kg) for 2 weeks. Data are generated from 5 mice per condition. (C) IHC analysis of EpCAM in lung metastasis detected in NOD/SCID mice SC injected with 2.5×10^5 HuH7 cells and 2.5×10^5 HLF cells. Metastasis was evaluated macro- and microscopically in the left and right lobes of the lung separately in each mouse ($n = 5$) (scale bar, 100 μm). (D) Cell motility of HuH7 cells cocultured with HuH7, HLF, or HLF cells with imatinib mesylate (10 μM) was monitored in a real-time manner by time-lapse image analysis. HuH7 and HLF cells were labeled with the lipophilic fluorescence tracer, DiI (indicated as red) or DiD (indicated as blue), and incubated in a μ-Slide eight-well chamber overnight. Silicone inserts were detached and the culture media replaced with Dulbecco's modified Eagle's medium containing 10% fetal bovine serum, including 0.1% dimethyl sulfoxide (DMSO) (control) or 10 μM of imatinib mesylate dissolved in DMSO (final concentration 0.1%). Immediately after the medium change, cells were cultured at 37°C in 5% CO_2 and time-lapse images were captured for 72 hours. (E) qPCR analysis of *TGFB1* in HuH7 (white bar), HLF (gray bar), and HLF cells pretreated with imatinib mesylate for 24 hours. (F) Smad3 and its phosphorylation evaluated by western blotting. HuH7 cells and HLF cells were harvested in cell culture inserts and treated with DMSO (0.1%) or imatinib mesylate (10 μM) for 24 hours. Cell culture inserts were washed with PBS, cocultured with HuH7 cells for 8 hours, and then removed. HuH7 cells were lysed using radioimmunoprecipitation assay buffer for western blotting. (A) HuH7 cells cocultured with HuH7 cells. (B) HuH7 cells cocultured with HLF cells. (C) HuH7 cells cocultured with HLF cells pretreated with imatinib mesylate.

HBV X may play a role in generating $EpCAM^+$ CSCs.[17] The role of hepatitis virus infection on the generation of CSCs is still unclear and should be clarified in future studies.

We were unable to confirm the tumorigenicity of $CD90^+$ cells in 13 of 15 HCCs, but we observed abundant $CD90^+$ cells in more-advanced HCCs by IHC (data not shown). Tumorigenic $CD90^+$ cells may emerge at a later stage of hepatocarcinogenesis, and the majority of $CD90^+$ cells in early HCCs may be cancer-associated VECs without tumorigenic capacity. Furthermore, we identified tumorigenic $CD90^+$ cells only from HBV-related HCCs, and a recent study suggested that expression of CD90 was associated with HBV infection.[16] We could not detect the small population of $CD90^+$ HuH7 and Hep3B cells reported on by Yang et al. However, because we identified a small population of $CD90^+$ HuH7 cells after treatment with 5-FU (manuscript in preparation), it is conceivable that different cellular stress statuses may explain the observed differences between our findings and those of Yang et al.

The majority of CSC markers discovered thus far are almost identical to those found in healthy tissue stem cells or embryonic stem cells. However, with regard to the liver, the characteristics of healthy hepatic stem/progenitor cells isolated using different stem cell markers are currently under investigation. A recent article examined the characteristics of $EpCAM^+$ and $CD90^+$ oval cells isolated from 2-acetylaminofluorene/partial hepatectomy or D-galactosamine-treated rats.[18] Interestingly, $EpCAM^+$ and $CD90^+$ oval cells represent two distinct populations: The former expresses classical oval cell markers, such as AFP, OV-1, and cytokeratin-19 (CK-19), whereas the latter expresses desmin and alpha smooth muscle actin, but not AFP, OV-1, or CK-19, which indicates that $CD90^+$ populations are more likely to be mesenchymal cells. Another study has demonstrated that mesenchymal cells can interact with HSCs to regulate cell-fate decision.[19] We found that $EpCAM^+$ and $CD90^+$ cells isolated from liver cancer are distinct in terms of gene- and protein-expression patterns in both primary liver cancers and cell lines. Furthermore, these distinct CSCs can interact to regulate the tumorigenicity and metastasis of HCC. Molecular characteristics of $EpCAM^+/CD90^+$ CSCs may potentially reflect the cellular context of healthy stem or progenitor cells.

Although our study strongly indicates that abundant $CD90^+$ cells in a tumor is a risk for distant metastasis in liver cancer, the cell identity and role of $CD90^+$ cells remains elusive. As our IHC, FACS, and xeno-transplantation assays revealed, some $CD90^+$ cells in liver cancer may be cancer-associated VECs or fibroblasts that cannot perpetuate in the xenograft. Recent findings have suggested the importance of stromal cells in tumorigenesis and cancer metastasis,[20-22] so it is possible that these cells may help TECs invade and intravasate into blood vessels, thus playing crucial roles in metastasis.

Another possibility is that $CD90^+$ cells are cancer cells with features of fibroblasts (having undergone EMT) or VECs (having undergone vasculogenic mimicry; VM) that can invade, intravasate, and metastasize cells to distant organs. Recently, two groups reported that a subset of tumor VECs originate from glioblastoma CSCs.[23,24] We successfully confirmed the tumorigenicity and metastatic capacity of $CD90^+$ cells that were morphologically identical to VECs from primary HCCs that could perpetuate in the xenograft. However, a recent study demonstrated that $CD90^+$ HCC cells express glypican-3, a marker detected in hepatic epithelial cells.[25] Further studies are warranted to clarify the nature and role of $CD90^+$ HCC cells.

In our study, $CD90^+$ cells expressed the endothelial marker, c-Kit, CD105, and VEGFR1, and a mesenchymal VEC morphology and high metastatic capacity were confirmed in both primary liver cancer and cell lines. We further confirmed that $CD90^+$ liver cancer cells showed chemosensitivity to imatinib mesylate, suggesting that cancer cells committed to mesenchymal endothelial lineages could be eradicated by the compound. Although imatinib mesylate treatment had little effect on the size of primary tumors originated from both $EpCAM^+$ and $CD90^+$ CSCs, it significantly suppressed lung metastasis *in vivo*. These data are consistent with a recent phase II study demonstrating the tolerable toxicity, but limited efficacy, of imatinib mesylate alone for unresectable HCC patients. Eligibility of imatinib mesylate for advanced HCC patients may be restricted to the HCC subtypes organized by $CD90^+$ CSCs with a highly metastatic capacity and VEC features. Therefore, a combination of compounds targeting $EpCAM^+$ tumorigenic CSCs as well as $CD90^+$ metastatic CSCs may be required for the eradication of HCC and should be tested in the future.

Acknowledgments: The authors thank Ms. Nami Nishiyama and Ms. Mikiko Nakamura for their excellent technical assistance.

References

1. Tsai WL, Chung RT. Viral hepatocarcinogenesis. Oncogene 2010;29: 2309-2324.

2. Chiba T, Kita K, Zheng YW, Yokosuka O, Saisho H, Iwama A, et al. Side population purified from hepatocellular carcinoma cells harbors cancer stem cell-like properties. HEPATOLOGY 2006;44:240-251.
3. Haraguchi N, Ishii H, Mimori K, Tanaka F, Ohkuma M, Kim HM, et al. CD13 is a therapeutic target in human liver cancer stem cells. J Clin Invest 2010;120:3326-3339.
4. Ma S, Tang KH, Chan YP, Lee TK, Kwan PS, Castilho A, et al. miR-130b promotes CD133(+) liver tumor-initiating cell growth and self-renewal via tumor protein 53-induced nuclear protein 1. Cell Stem Cell 2010;7:694-707.
5. Yang ZF, Ho DW, Ng MN, Lau CK, Yu WC, Ngai P, et al. Significance of CD90+ cancer stem cells in human liver cancer. Cancer Cell 2008;13:153-166.
6. Zen Y, Fujii T, Yoshikawa S, Takamura H, Tani T, Ohta T, Nakanuma Y. Histological and culture studies with respect to ABCG2 expression support the existence of a cancer cell hierarchy in human hepatocellular carcinoma. Am J Pathol 2007;170:1750-1762.
7. Lee TK, Castilho A, Cheung VC, Tang KH, Ma S, Ng IO. CD24(+) liver tumor-initiating cells drive self-renewal and tumor initiation through STAT3-mediated NANOG regulation. Cell Stem Cell 2011;9: 50-63.
8. Yamashita T, Budhu A, Forgues M, Wang XW. Activation of hepatic stem cell marker EpCAM by Wnt-beta-catenin signaling in hepatocellular carcinoma. Cancer Res 2007;67:10831-10839.
9. Yamashita T, Forgues M, Wang W, Kim JW, Ye Q, Jia H, et al. EpCAM and alpha-fetoprotein expression defines novel prognostic subtypes of hepatocellular carcinoma. Cancer Res 2008;68:1451-1461.
10. Yamashita T, Ji J, Budhu A, Forgues M, Yang W, Wang HY, et al. EpCAM-positive hepatocellular carcinoma cells are tumor-initiating cells with stem/progenitor cell features. Gastroenterology 2009;136: 1012-1024.
11. Ma S, Chan KW, Hu L, Lee TK, Wo JY, Ng IO, et al. Identification and characterization of tumorigenic liver cancer stem/progenitor cells. Gastroenterology 2007;132:2542-2556.
12. Heffelfinger SC, Hawkins HH, Barrish J, Taylor L, Darlington GJ. SK HEP-1: a human cell line of endothelial origin. In Vitro Cell Dev Biol 1992;28A:136-142.
13. Ishimoto T, Nagano O, Yae T, Tamada M, Motohara T, Oshima H, et al. CD44 variant regulates redox status in cancer cells by stabilizing the xCT subunit of system xc(-) and thereby promotes tumor growth. Cancer Cell 2011;19:387-400.
14. Ramadori G, Fuzesi L, Grabbe E, Pieler T, Armbrust T. Successful treatment of hepatocellular carcinoma with the tyrosine kinase inhibitor imatinib in a patient with liver cirrhosis. Anticancer Drugs 2004;15: 405-409.
15. Kim H, Choi GH, Na DC, Ahn EY, Kim GI, Lee JE, et al. Human hepatocellular carcinomas with "Stemness"-related marker expression: keratin 19 expression and a poor prognosis. HEPATOLOGY 2011;54: 1707-1717.
16. Lu JW, Chang JG, Yeh KT, Chen RM, Tsai JJ, Hu RM. Overexpression of Thy1/CD90 in human hepatocellular carcinoma is associated with HBV infection and poor prognosis. Acta Histochem 2011;113: 833-838.
17. Arzumanyan A, Friedman T, Ng IO, Clayton MM, Lian Z, Feitelson MA. Does the hepatitis B antigen HBx promote the appearance of liver cancer stem cells? Cancer Res 2011;71:3701-3708.
18. Yovchev MI, Grozdanov PN, Zhou H, Racherla H, Guha C, Dabeva MD. Identification of adult hepatic progenitor cells capable of repopulating injured rat liver. HEPATOLOGY 2008;47:636-647.
19. Wang Y, Yao HL, Cui CB, Wauthier E, Barbier C, Costello MJ, et al. Paracrine signals from mesenchymal cell populations govern the expansion and differentiation of human hepatic stem cells to adult liver fates. HEPATOLOGY 2010;52:1443-1454.
20. Dome B, Timar J, Ladanyi A, Paku S, Renyi-Vamos F, Klepetko W, et al. Circulating endothelial cells, bone marrow-derived endothelial progenitor cells and proangiogenic hematopoietic cells in cancer: from biology to therapy. Crit Rev Oncol Hematol 2009;69:108-124.
21. Karnoub AE, Dash AB, Vo AP, Sullivan A, Brooks MW, Bell GW, et al. Mesenchymal stem cells within tumour stroma promote breast cancer metastasis. Nature 2007;449:557-563.
22. Mishra PJ, Humeniuk R, Medina DJ, Alexe G, Mesirov JP, Ganesan S, et al. Carcinoma-associated fibroblast-like differentiation of human mesenchymal stem cells. Cancer Res 2008;68:4331-4339.
23. Ricci-Vitiani L, Pallini R, Biffoni M, Todaro M, Invernici G, Cenci T, et al. Tumour vascularization via endothelial differentiation of glioblastoma stem-like cells. Nature 2010;468:824-828.
24. Wang R, Chadalavada K, Wilshire J, Kowalik U, Hovinga KE, Geber A, et al. Glioblastoma stem-like cells give rise to tumour endothelium. Nature 2010;468:829-833.
25. Ho DW, Yang ZF, Yi K, Lam CT, Ng MN, Yu WC, et al. Gene expression profiling of liver cancer stem cells by RNA-sequencing. PLoS One 2012;7:e37159.

Biochemical and Biophysical Research Communications 428 (2012) 36–43

Contents lists available at SciVerse ScienceDirect

Biochemical and Biophysical Research Communications

journal homepage: www.elsevier.com/locate/ybbrc

Association of changes in the gene expression profile of blood cells with the local tumor inflammatory response in a murine tumor model

Yoshio Sakai [a,b], Isamu Tatsumi [c], Mami Higashimoto [c], Akihiro Seki [c], Alessandro Nasti [c], Keiko Yoshida [c], Kazunori Kawaguchi [c], Takashi Wada [b], Masao Honda [c], Takuya Komura [c], Shuichi Kaneko [a,c,*]

[a] Department of Gastroenterology, Kanazawa University, Japan
[b] Department of Laboratory Medicine, Kanazawa University, Japan
[c] Disease Control and Homeostasis, Kanazawa University, Japan

ARTICLE INFO

Article history:
Received 28 September 2012
Available online 9 October 2012

Keywords:
Peripheral blood cell
Gene expression profile
Local tumor inflammation

ABSTRACT

Cancer tissue is frequently associated with the host inflammatory response, which involves blood cells. Using DNA microarrays, we examined the gene expression profiles of blood and tumors in a murine subcutaneous hepatocellular carcinoma model, in which tumors develop during the initial 10 days and then diminish and disappear by day 25 after implantation. Immunohistochemical and gene expression analysis indicated that tumor tissues were associated with an active immune response, particularly the CD4+ T cell-mediated immune response, on day 10. The genes commonly up-regulated in blood and the fraction enriched with tumor-associated inflammatory cells on day 10 also suggested the involvement of CD4+ T cells. Unsupervised hierarchical clustering analysis of gene expression of peripheral blood cells on days 0, 10, 15, 20, and 25 indicated two major clusters: the tumor-existence cluster on days 10, 15, and 20, and the tumor-free cluster on days 0 and 25. Additionally, sub-clusters were detected on each day. These results suggest that the gene expression profile of whole blood cells is affected by the local tumor condition, and is associated with the local host immune response. Its analysis will facilitate exploration of the underlying important features of the host immune response to tumors.

1. Introduction

Cancer is one of the most serious diseases if early diagnosis fails or in cases of recurrence after radical treatment [1]. Therefore, elucidating the detailed biological features of cancer is important for development of new useful diagnostic and therapeutic methods to improve the prognosis of cancer patients [2]. Immunity is an important physiological homeostasis system that protects the host from various diseases. Cancer is frequently associated with the immune reaction of the host [3], although cancer originates from self tissues. Peripheral blood contains a substantial number of immune-mediating cells that can respond to affected tissues or pathogens; therefore, they are a crucial population that reacts to diseases, including cancer, to protect the host.

Whereas the host responds to lesions in the body, the blood reveals consequent characteristic manifestations—*i.e.*, neutrophilia for bacterial infection [4] or leukopenia for viral infection [5]. In the host with cancer, circulating blood contains characteristic immune-mediating cells—*e.g.*, cytotoxic T cells [6,7] and regulatory T cells [8,9]—due to the immune response to the disease. Assessment of these immune-mediating cells in blood is useful for evaluations of prognosis and therapeutic effect because cytotoxic T cells play a role in cancer eradication, whereas regulatory T cells inhibit the host anti-cancer immune response. Therefore, assessment of blood cells is a useful approach to evaluating host immune status in various diseases, including cancer [10,11].

Whole-genome expression analysis using DNA microarray technology allows examination of various biological processes [12–14]. We have reported previously that peripheral blood exhibited a characteristic gene expression profile in cancer [15,16]. Although these studies suggest the usefulness of peripheral blood gene-expression analysis for exploration of the pathophysiological features/conditions of cancer, how the altered gene expression profile of blood cells contributes to understanding of the condition of individuals with cancer remains unknown.

We have established subcutaneous hepatocellular carcinoma (HCC) murine models that show the unique course of cancer: transient development followed by diminishing. This course was mediated by the immune response, particularly CD4+ T cells. Altered gene expression in whole blood cells as well as local

Abbreviation: HCC, hepatocellular carcinoma.

* Corresponding author. Address: Department of Gastroenterology, Kanazawa University, 13-1 Takara-machi, Kanazawa, Ishikawa 920-8641, Japan. Fax: +81 76 234 4250.
E-mail address: skaneko@m-kanazawa.jp (S. Kaneko).

0006-291X/$ - see front matter © 2012 Elsevier Inc. All rights reserved.
http://dx.doi.org/10.1016/j.bbrc.2012.10.004

tumor-associated inflammatory cells implied CD4+ T cell-involvement. Furthermore, the gene expression profiles of blood differed depending on the condition of cancer tissues, suggesting that blood-cell gene expression is associated with tumor condition and that its analysis is useful for investigation of the biological features of the host immune response to cancer.

2. Materials and methods

2.1. Cell culture

Hepa1-6 (ATCC, Manassas, VA), an established murine HCC cell line, was maintained in Dulbecco's modified Eagle's medium (Life Technologies, Carlsbad, CA) supplemented with 10% heat-inactivated fetal bovine serum (Life Technologies).

2.2. Subcutaneous HCC murine model

C57Bl/6 female mice (8 weeks old; Charles River Laboratories, Yokohama, Japan) or BALB/c athymic female mice (8 weeks old) were injected subcutaneously with 1×10^7 Hepa1-6 cells. Tumor size was monitored and the volume was calculated using the following formula:

$$\text{Tumor volume}(\text{mm}^3) = (\text{the shortest diameter})^2 \times (\text{the longest diameter})/2$$

Animal experiments were approved by the institutional review board.

2.3. Immunohistochemistry

Hepa1-6 subcutaneous tumor tissues were removed and embedded in optimal cutting temperature compound (Sakura Finetek, Torrance, CA), snap-frozen in liquid nitrogen, and cryostat-sectioned. Tissues were also fixed with neutral-buffered formalin, embedded in paraffin, cut into 4-μm sections, mounted on microscope slides, and stained with hematoxylin and eosin. Cryostat sections of frozen tissues were fixed in cold acetone, and endogenous biotin/avidin in the tissue specimens were blocked using a blocking kit (Vector Laboratories, Inc., Burlingame, CA). Slides were incubated with the appropriately diluted primary antibodies, anti-mouse CD4, CD8, CD11b (BD Pharmingen, Sparks, MD), and Gr-1 (eBioscience, San Diego, CA), respectively. The reactions were visualized using EnVision kits (DAKO, Glostrup, Denmark), followed by counterstaining with hematoxylin.

2.4. RNA isolation

Blood was obtained by retro-orbital venipuncture from mice and immediately stored as RNAlater aliquots (Ambion, Austin, TX). Total RNA of the obtained whole blood was extracted using the Mouse RiboPure™-Blood RNA Isolation Kit (Ambion), according to the manufacturer's protocol. A portion of Hepa1-6 tumor tissues was obtained and stored in RNAlater, followed by RNA isolation using the RNeasy Mini Kit (QIAGEN, Tokyo, Japan). The tumor fraction enriched with tumor-associated inflammatory cells was obtained using Histopaque®. Briefly, tumor tissues were minced and overlaid on the Histopaque® aliquot. After centrifugation, the visible separated monolayer was collected. RNA was isolated from the collected fraction using the microRNA Isolation Kit (Stratagene, La Jolla, CA), according to the manufacturer's protocol. The quality of purified RNA was analyzed using an Agilent 2100 Bioanalyzer (Agilent Technologies, Santa Clara, CA).

2.5. Gene expression analysis by DNA microarray and data analysis

Isolated RNA was amplified and labeled with Cy5 using the Quick Amp Labeling Kit (Agilent Technologies) according to the manufacturer's protocol. For reference, RNA isolated from the blood of normal C57Bl/6 or BALB/c athymic female mice was amplified and labeled with Cy3. The labeled objective and reference cRNA was mixed and hybridized using the Whole Mouse Genome 4×44K Array kit (Agilent Technologies). The slide was scanned using a DNA Microarray Scanner (Model G2505B; Agilent Technologies). Microarray data were deposited in NBCI Gene Expression Omnibus (GSE ID: GSE 39075).

Gene expression analysis was performed using the GeneSpring analysis software (Agilent Technologies). Each measurement was divided by the 75th percentile of all measurements in that sample at per chip normalization. Hierarchical clustering and principal component analysis of gene expression were performed. Welch's *t*-test with Benjamini and Hochberg's false discovery rate were used to identify genes that were differentially expressed in the groups of interest. Analysis of biological processes and networks was performed using the MetaCore software suite (GeneGo, Carlsbad, CA).

3. Results

3.1. Subcutaneous Hepa1-6 HCC cells in C57Bl/6 mice grew transiently and subsequently diminished due to the T-cell immune response

Hepa1-6 murine HCC cells were subcutaneously injected into C57Bl/6 female mice and tumor size was monitored. Until day 10, implanted Hepa1-6 cells proliferated continuously, forming a consistent tumor. From days 10 to 15, tumor size started to decrease, and the established tumors were completely eradicated by day 25 (Fig. 1A). In contrast, when Hepa1-6 cells were subcutaneously injected into BALB/c athymic mice, which were deleted of most, if not all, T cells due to the lack of a thymus, tumor tissues were established and continued to grow during the 37-day observation period without stabilization or diminishment (Fig. 1B). Histologically, tumors in C57Bl/6 mice obtained on days 10 and 15 were filled with viable Hepa1-6 cells (Fig. 1C). Tumor tissues obtained on day 20 showed fibrous tissues with few viable Hepa1-6 cells (Fig. 1C). Immunohistochemical analysis of immune-mediating cells in tumors showed that a substantial number of CD4+ T cells were found on day 10, the frequency of which was reduced after day 15 (Fig. 1D). In contrast, fewer CD8+ T cells were detected during any phase (Fig. 1D). CD11b+ and Gr-1+ cells were observed during all tumor phases (Fig. 1D). We also examined infiltrating inflammatory cells in the Hepa1-6 tumors after 10 days' growth in athymic mice. In contrast to the intensively infiltrating CD4+ T cells in Hepa1-6 tumors in C57Bl/6 mice on day 10 (Fig. 1D), few CD4+ T cells and no CD8+ T cells were observed in Hepa1-6 tumors from athymic mice (Supplementary Fig. S1). CD11b+ cells were diffusely present and a substantial number of infiltrating Gr-1+ cells were found (Supplementary Fig. S1). These results suggest that the characteristic feature of the immune response in subcutaneous Hepa1-6 tumors of C57Bl/6 mice on day 10 was CD4+ T cell-involvement.

3.2. Gene expression profiles of Hepa1-6 tumors on days 10 and 15

Tumors established in C57Bl/6 on days 10 and 15 revealed a similar appearance microscopically (Fig. 1C), whereas more CD4+ T cells infiltrated into tumors on day 10 than on day 15. To compare the molecular biological features of tumors on days 10 ($n = 3$) and 15 ($n = 3$), we assessed gene expression profiles using

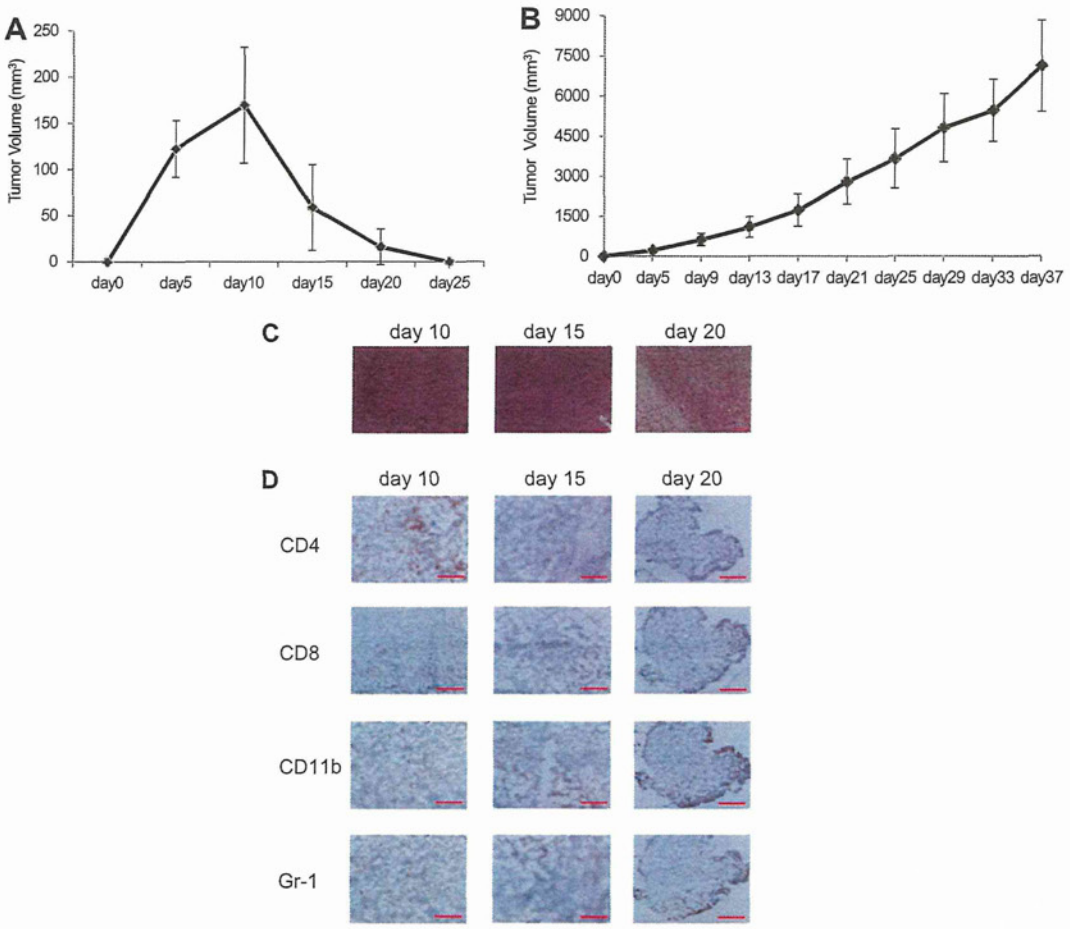

Fig. 1. The subcutaneous Hepa1-6 tumor model. Ten million Hepa1-6 HCC cells were subcutaneously inoculated into C57Bl/6 mice or Balb/c athymic mice. The size of tumors was monitored and tumor tissues were examined histologically as well as immunohistochemically. (A) Tumor growth in C57Bl/6 mice. (B) Tumor growth in Balb/c athymic mice. Bars, standard errors. (C) Histological features of inoculated Hepa1-6 subcutaneous tumors in C57Bl/6 mice on days 10, 15, and 25. Hematoxylin and eosin staining. Bars, 100 μm. (D) Immunohistochemical analysis of subcutaneous Hepa1-6 tumors in C57BL/6 mice on days 10, 15 and 25. Bars, 200 μm.

DNA microarrays. We identified 118 gene probes twofold differentially expressed between days 10 and 15 with $p < 0.05$ (Supplementary Table S1). Unsupervised hierarchical clustering and principal component analysis showed formation of two complete clusters on days 10 and 15 (Fig. 2). Network analysis of these 118 genes probes showed that regulation of T-cell proliferation was associated with the Stat5b, Stat5a, Jak2, Cyclin D1, and androgen receptor genes, whereas muscle filament sliding was associated with the Myh4, Myosin-IIA, Prelid2, Acta1, and Actc genes (Table 1). Thus, the T-cell immune responses to tumors on days 10 and 15 were markedly different.

3.3. Genes up-regulated in both blood and tumor-associated inflammatory cells were associated with local tumor conditions

The results shown above suggested that T cells, particularly CD4+ T cells, played an important role in the immune reaction to Hepa1-6 tumors in C57Bl/6 mice on day 10. To evaluate the relevance of local tumor inflammation and blood cells, we determined the genes whose expression was altered in the blood and tumor fraction enriched with tumor-associated inflammatory cells of C57Bl/6 mice ($n = 8$) or Balb/c athymic mice ($n = 3$) with Hepa1-6 tumors on day 10. We identified 127 genes whose expression was commonly twofold up-regulated ($p < 0.05$) between the tumor fraction enriched with tumor-associated inflammatory cells and whole blood cells in C57Bl/6 mice (Supplementary Table S2). The characteristic features involved a network that involved the C3g, IL-2r alpha chain, Shh, CD4, and Tgf-alpha genes (Table 2 and Fig. 3). Other networks were also observed to involve CD4: the network that involved Mkl2 (Mrtf-b), CD4, Dysstrophin, Pthr1, and Col1a2 and that involving CD4, Cdk1 (p34), iNOS, Tmem107, Dlx4 (Bp1). Sixty-five genes whose expression was commonly twofold up-regulated ($p < 0.05$) between the tumor fraction enriched with tumor-associated inflammatory cells and whole blood cells of athymic mice ($n = 3$) on day 10 were identified (Supplementary Table S3). Gene ontology processes for these genes included transcription, macromolecule metabolic process, regulation of multicellular organismal process, and development-related process, suggesting a role for local tumor-associated inflammatory cells in tumor development (Supplementary Table S4).

Thus, the biological features of genes up-regulated in both local tumor-associated inflammatory cells and blood cells suggested an underlying host CD4+ T cell-mediated immune response to tumors in C57Bl/6 mice, suggesting that the altered gene expression profile in systemically circulating blood cells reflected the local tumor conditions.

3.4. Whole peripheral-blood gene expression profiles were associated with tumor condition

Genes whose expression was altered in the blood of mice with Hepa1-6 tumors implied inflammation local to the tumor. We next

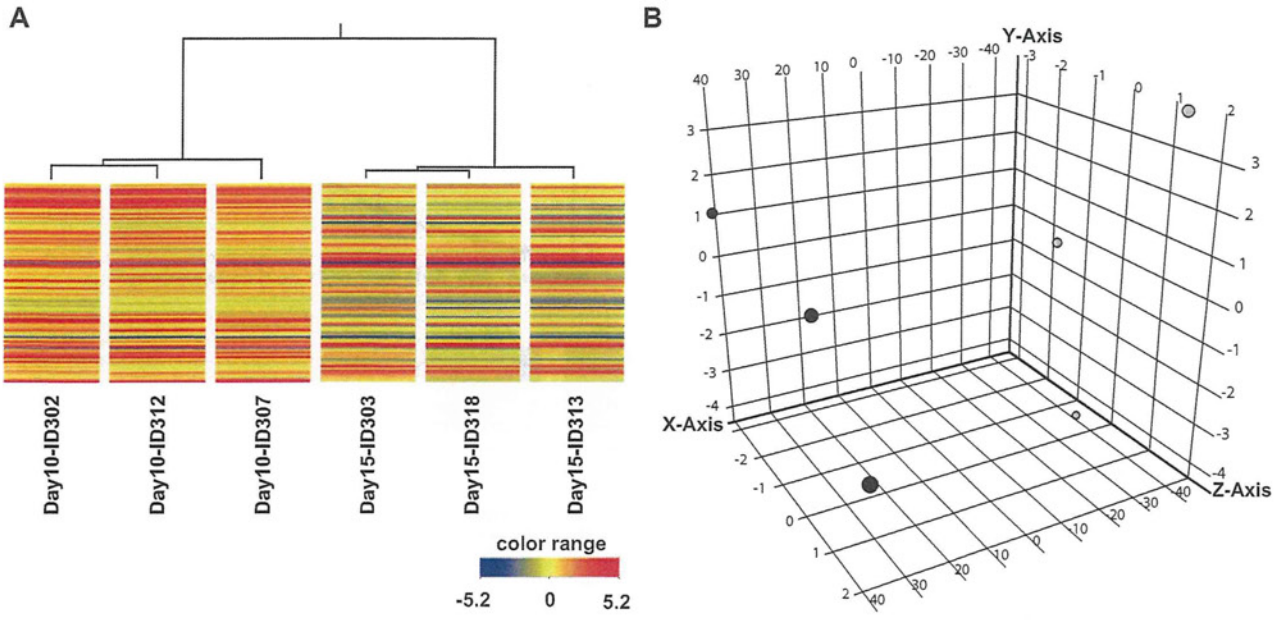

Fig. 2. Hierarchical clustering and principal component analysis of gene expression in subcutaneous Hepa1-6 tumors. Tumor tissues were obtained 10 and 15 days after subcutaneous inoculation of Hepa1-6 cells in C57Bl/6 mice and gene expression levels were evaluated by microarray. Unsupervised clustering (A) and principal component analysis (B) were performed using 118 probes specific for genes whose expression was significantly different at twofold. Filled circles, day 10. Gray circles, day 15.

Table 1
Networks for genes whose expression in tumors of C57Bl/6 mice was differetially expressed between day 10 and day 15.

Network	*p*-Value	GO processes
Stat5b, Androgen receptor, Stat5a, Jak2, Cyclin D1	0.0672	Positive regulation of activated T cell proliferation, cellular response to chemical stimulus, positive regulation of cell proliferation, regulation of activated T cell proliferation, response to hormone stimulus
Myh4, Myosin-IIA, Prelid2, Acta1, Actc	2.29×10^{-19}	Muscle filament sliding, actin-myosin filament sliding, actin-mediated cell contraction, actin filament-based movement, muscle system process
Rev-Eerb-b, Comp, Substance P receptor, Kcrm, Lingo1	7.02×10^{-15}	Regulation of multicellular organismal process, response to external stimulus, intracellular signal transduction, transmembrane receptor protein tyrosine kinase signaling pathway, multicellular organismal process
Bmal1, Stat5b, Pdgf-r-alpha, CD20, Dbp	7.26×10^{-13}	Positive regulation of transcription from RNA polymerase II promoter, regulation of transcription from RNA polymerase II promoter, positive regulation of gene expression, positive regulation of transcription, DNA-dependent, regulation of cellular biosynthetic process
Krt25, Keratin, type I cytoskeletal 25	0.00145	Intermediate filament organization, hair follicle morphogenesis, intermediate filament cytoskeleton organization, intermediate filament-based process, epidermis morphogenesis

explored how the gene expression profiles of whole blood cells changed with altering tumor conditions in mice with Hepa1-6 tumors. Blood was collected from C57Bl/6 mice before and 10, 15, 20, and 25 days after Hepa1-6 subcutaneous implantation, and then total RNA was isolated for gene expression analysis. The number of gene probes twofold up-regulated in the blood of mice with tumors compared with that of mice on day 0 was 968 on day 10 (Supplementary Table S5), 945 on day 15 (Supplementary Table S6), 53 on day 20 (Supplementary Table S7), and 14 on day 25 (Supplementary Table S8), and 418, 338, 61, and 134 gene probes, respectively, were down-regulated (Supplementary Tables S9, S10, S11 and S12). Unsupervised analysis of gene expression using 23,326 DNA microarray gene of that passed quality checking showed two major clusters, one associated with tumor presence on days 10, 15, and 20 (the tumor existence cluster), and the other to being tumor-free on days 0 and 25 (the tumor-free cluster), with minor discernible clusters depending on each day (Fig. 4A). Principal component analysis also revealed that the gene expression profile of each mouse differed depending on the day (Fig. 4B). We identified that 1525 genes probes was the union of 968 and 945 up-regulated genes probes on day 10 and day 15, indicating that 388 genes probes were commonly up-regulated. Despite considerable number of commonly up-regulated genes probes, clustering analysis using 1525 genes probes for gene expression profiles in blood on day 10 and day 15 formed two complete clusters discerning each day, suggesting that gene expression profile of blood was changing during the initiating phases of tumor diminishment. A pathway map analysis was performed on 968 and 945 genes whose expression was up-regulated on days 10 and 15, respectively. Development-related and cytoskeleton-remodeling pathways were the characteristic features of both groups (Supplementary Tables S13 and S14). Pathway maps for cell adhesion—integrin-mediated cell adhesion and migration, CCR4-induced leukocyte adhesion, plasmin signaling, and endothelial cell contacts by non-junctional mechanisms—were the prominent features of up-regulated genes on day 15 (Supplementary Table S14), suggesting enhanced involvement of tissue remodeling. We also analyzed the biological process features of genes differentially expressed between the tumor existence and tumor-free clusters. The number of gene probes whose expression was twofold up-regulated in the tumor existence cluster ($p < 0.05$) was 673, whereas 17 gene probes were down-regulated. The characteristic biological process networks indicated by these 673 gene probes were cytoskeleton, development, cell cycle, apoptosis, and cell adhesion (Supplemen-

Table 2
Networks for genes whose expression was commonly up-regulated in the tumor fraction enriched with tumor-associated inflammatory cells and blood of C57Bl/6 mice on day 10.

Network	*p*-Value	Gene ontology processes
C3g, Il-2r alpha chain, Shh, CD4, Tgf-alpha	9.26×10^{-22}	Positive regulation of cell proliferation, regulation of macromolecule metabolic process, cell proliferation, positive regulation of cellular process, regulation of cell proliferation
Cdk1 (p34), Aggrecan, Sox9, PNPase(old-35), Nyd-sp26	3.85×10^{-17}	Regulation of cell proliferation, generation of neurons, cellular developmental process, anatomical structure morphogenesis, neurogenesis
Nanos2, Nanos homolog 2	0.00143	Germ-line stem cell maintenance, negative regulation of meiosis, regulation of meiosis, regulation of meiotic cell cycle, stem cell maintenance
Wdr59, WD repeat-containing protein 59,	0.00143	Biological_process
Cdk1 (p34), Alk, Racgap1, Fibrinogen beta, Mmd	9.51×10^{-11}	Blood coagulation, coagulation, hemostasis, cytoskeleton organization, wound healing
Mkl2(Mrtf-b), CD4, Dystrophin, Pthr1, Col1a2	9.51×10^{-11}	Positive regulation of protein metabolic process, positive regulation of cellular metabolic process, positive regulation of metabolic process, regulation of cell proliferation, positive regulation of cellular process
Dnah12, Dynein, axonemal, heavy chains	0.00286	Microtubule-based movement, ATP catabolic process, ATP metabolic process, microtubule-based process, purine ribonucleoside triphosphate catabolic process
CD4, Cdk1 (p34), iNOS, Tmem107, Dlx4 (Bp1)	9.63×10^{-9}	Positive regulation of cellular metabolic process, interspecies interaction between organisms, positive regulation of metabolic process, positive regulation of macromolecule metabolic process, positive regulation of developmental process
Cdk1 (p34), Pthr1, Centg2, Bex2, Bex1	1.07×10^{-8}	G-protein signaling, coupled to cAMP nucleotide second messenger, cAMP-mediated signaling, G-protein signaling, coupled to cyclic nucleotide second messenger, cyclic-nucleotide-mediated signaling, regulation of catalytic activity
Fam33a, Mkl2(Mrtf-b), Cdk1 (p34), Tank, Pitx2	1.07×10^{-8}	Positive regulation of macromolecule metabolic process, positive regulation of cellular metabolic process, regulation of cellular metabolic process, cell cycle, positive regulation of metabolic process

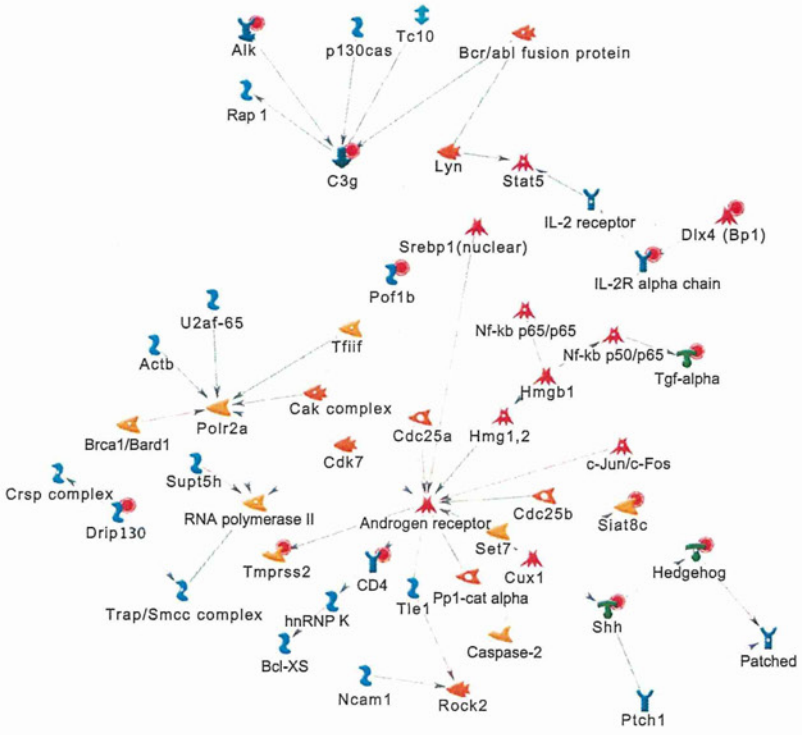

Fig. 3. Network depicting the involvement of C3G, IL-2R alpha chain, SHH, CD4, and TGF-alpha genes. Ten million Hepa1-6 cells were subcutaneously inoculated in C57Bl/6 mice. Blood and tumor tissues were obtained on day 10. Gene expression levels in blood and the fraction enriched with tumor-associated inflammatory cells were assessed by DNA microarray. One-hundred and twenty-seven genes were commonly up-regulated at twofold in blood and the tumor fraction enriched with tumor-associated inflammatory cells, and were related to the gene network that consisted of C3G, IL-2R alpha chain, SHH, CD4, and TGF-alpha plus related genes.

tary Table S15), implying the dynamic role of blood cells in immobilization and cellular kinesis, indicative of tissue remodeling, of tumors associated with the active immune response of the C57Bl/6 mouse.

We also examined whole blood gene expression profiles of BALB/c athymic mice with Hepa1-6 tumors on day 10 compared with that before inoculation of Hepa1-6 cells. Unsupervised clustering analysis of gene expression using 15583 gene probes that passed quality checking showed two clusters, clearly distinguishing between the tumor-existence and tumor-free conditions (Supplementary Fig. S2A). Principal component analysis showed that the gene expression profiles on days 0 and 10 tended to gather depending on the day (Supplementary Fig. S2B). We found that expression of 962 gene probes was up-regulated on day 10 compared with day 0. Pathway map analysis of the 962 gene probes revealed cell kinetics involving transcription, the cell cycle, and cell

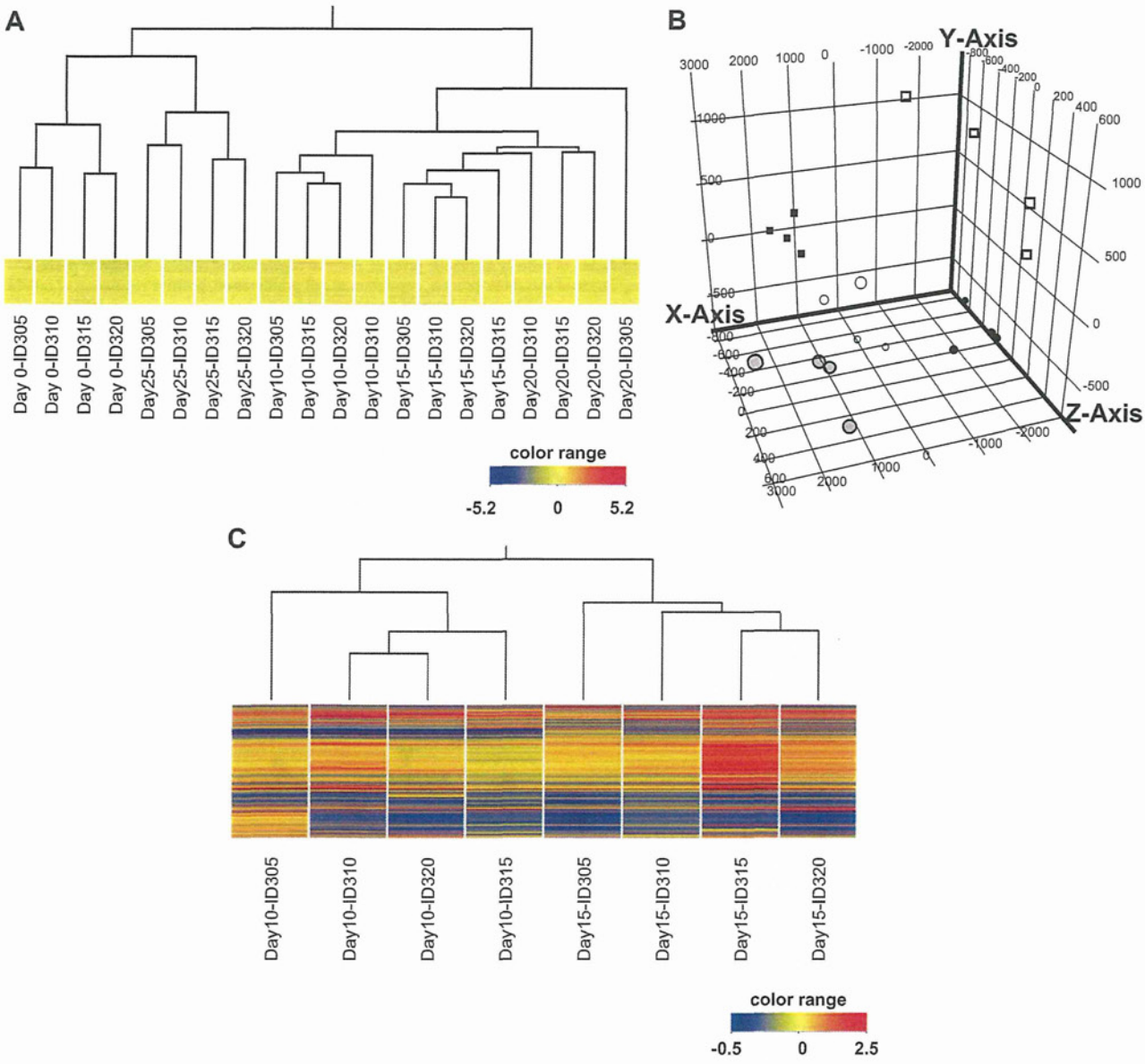

Fig. 4. Hierarchical clustering and principal component analysis of gene expression levels in blood obtained from C57Bl/6 mice inoculated subcutaneously with Hepa1-6 cells. RNA was extracted from the blood of C57Bl/6 mice inoculated with Hepa1-6 cells on days 0, 10, 15, 20, and 25, followed by gene expression analysis by DNA microarray. (A) Unsupervised hierarchical clustering and (B) principal component analysis of gene expression levels on day 0, 10, 15, 20, and 25 using all gene probes that passed a quality check. Open rectangle, day 0; filled rectangle, day 25; filled circle, day 10; gray circle, day 15; open circle, day 20. (C) Unsupervised hierarchical clustering of gene expression levels on day 10 and day 15 using the 1525 union genes probes up-regulated on day 10 and day 15.

adhesion (Supplementary Table S16), suggesting a relationship between blood cells and locally proliferating tumor cells that were inoculated subcutaneously. Thus, the gene expression profiles of whole blood cells in mice with tumors were altered depending on the local tumor conditions.

4. Discussion

The subcutaneously inoculated Hepa1-6 cells in C57Bl/6 mice demonstrated the unique course of tumor development/diminishment. Eradication of tumors was mediated by the T-cell immune response, particularly CD4+ T cells. Interestingly, genes up-regulated in both whole blood and the tumor fraction enriched with tumor-associated inflammatory cells on day 10 indicated a biological network involving CD4+ T cells, suggesting that gene expression alteration of whole blood cells was associated in part with the local inflammatory response to tumor tissues. Additionally, the gene expression profiles of whole blood cells in mice with Hepa1-6 tumors were associated with the tumor condition, and their biological features during tumor existence were suggestive of tissue remodeling-related processes.

The genes commonly affected in both blood cells and the tumor fraction enriched with tumor-associated inflammatory cells in C57Bl/6 mice suggested a biological network involving CD4+ T cells. Thus, CD4+ T cells may contribute to the altered blood gene expression profile on day 10. However, the blood gene expression profile of athymic mice with Hepa1-6 tumors was discernible from that of tumor-free mice, suggesting the involvement of other immune-mediating cells in the altered blood gene expression profile.

The gene expression profiles of whole blood cells of C57Bl/6 mice with tumors indicated biological processes related to tissue remodeling, such as development, cell adhesion, and the cytoskeleton. A fraction of circulating blood cells are involved in tissue remodeling/repair, such as monocytes/macrophages [17–19]. Thus, some blood cells likely contributed to these biological features as a consequence of tumor formation. The mechanism(s) underlying the association between blood gene expression profile and tumor condition should be determined.

We reported previously that features of the gene expression profile of peripheral blood mononuclear cells of HCC patients are shared with local inflammatory cells of HCC tissues [16]. In that analysis, the shared biological features were characterized by the local immune responses of the host to tumor tissues, tumor microenvironment—such as antigen presentation, response to hypoxia, and oxidative stress—ubiquitin-proteasomal proteolysis, mRNA processing, and the cell cycle. Peripheral blood mononuclear cells are devoid of cell types such as polymorphonuclear cells; therefore, the collected peripheral blood mononuclear cell populations rather contain inflammatory cells that are the major players in cancer immunity: the antigen-presenting cell population (monocytes/macrophages and dendritic cells), and the lymphocyte population (T and B cells) [20]. In the current study, gene expression of peripheral blood involved all cell populations therein. However, the genes up-regulated in both blood and the tumor fraction enriched with tumor-associated inflammatory cells suggested the importance of local tumor-associated CD4+ T cells, which played an important role in the C57Bl/6 mouse Hepa1-6 tumor model. Blood gene expression profiles of C57Bl/6 and athymic mice with Hepa1-6 tumors also depended on the presence and/or condition of a tumor. However, Gr-1+ cells were the major local inflammatory cells in the Hepa1-6 tumors of athymic mice. Because the network of genes up-regulated in blood and tumor-associated inflammatory cells in the athymic mouse model involved cellular kinetics and development, not directly suggestive of Gr-1+ cells, the role of local Gr-1+ cells in the alteration of blood gene expression profiles is unclear. Further studies should determine how immune-mediating cells in both blood and local tumor-infiltrating inflammatory cell populations alter blood gene expression depending on tumor condition.

The immune reaction of the host to cancer is complex: natural killer cells are well-characterized anti-cancer immune cells [21], and the innate immune system is represented by monocyte/macrophages [22]. In terms of acquired immunity, Th1 cells and cytotoxic T cells are known to be important due to the presence of antigen-presenting dendritic cells [23]. In contrast, the contradictory immune response is present concomitantly; this involves, for instance, regulatory T cells [8,9]. When anti-cancer immune cells predominate, cancer tissues will diminish. Conversely, when immune cells that work as suppressors of anti-cancer immunity are the major effectors, the tumor tissue will continue to grow. Thus, qualitative elucidation of host immune status is extremely important for assessing both prognosis and therapeutic efficacy. Blood gene expression analysis has been investigated extensively and has been shown to be useful in terms of diagnosis, prediction of a therapeutic effect, or prognosis in, for example, renal cell carcinoma [24], breast cancer [25], and digestive disease cancers [26]. Our data suggest that the blood gene expression profile of a murine cancer model was associated with the local tumor condition. The utility of blood cell gene expression profiling for further elucidation of the overall immune condition in terms of the presence of immune-mediating cell types should be investigated.

In conclusion, we observed that gene expression features of peripheral blood cells were altered depending on tumor condition. Additionally, biological features associated with CD4+ T cells, which play a pivotal role in Hepa1-6 C57Bl/6 tumor models, were implicated in the gene expression profiles common to both blood and tumor-infiltrating inflammatory cells. Further studies are needed to understand the systemic effect of cancer on blood gene expression profiles in other cancer-related conditions —*e.g.*, recurrent cancer or vaccination—for development of both novel diagnostic tools and effective treatments.

Acknowledgment

This work was supported in part by a subsidy of the Ministry of Education, Culture, Sports, Science and Technology, Japan.

Appendix A. Supplementary data

Supplementary data associated with this article can be found, in the online version, at http://dx.doi.org/10.1016/j.bbrc.2012.10.004.

References

[1] B.K. Edwards, E. Ward, B.A. Kohler, C. Eheman, A.G. Zauber, R.N. Anderson, A. Jemal, M.J. Schymura, I. Lansdorp-Vogelaar, L.C. Seeff, M. van Ballegooijen, S.L. Goede, L.A. Ries, Annual report to the nation on the status of cancer, 1975–2006, featuring colorectal cancer trends and impact of interventions (risk factors, screening, and treatment) to reduce future rates, Cancer 116 (2010) 544–573.
[2] S. De Masi, M.E. Tosti, A. Mele, Screening for hepatocellular carcinoma, Dig. Liver Dis. 37 (2005) 260–268.
[3] K. Nosho, Y. Baba, N. Tanaka, K. Shima, M. Hayashi, J.A. Meyerhardt, E. Giovannucci, G. Dranoff, C.S. Fuchs, S. Ogino, Tumour-infiltrating T-cell subsets, molecular changes in colorectal cancer, and prognosis: cohort study and literature review, J. Pathol. 222 (2010) 350–366.
[4] M.J. Delano, K.M. Kelly-Scumpia, T.C. Thayer, R.D. Winfield, P.O. Scumpia, A.G. Cuenca, P.B. Harrington, K.A. O'Malley, E. Warner, S. Gabrilovich, C.E. Mathews, D. Laface, P.G. Heyworth, R. Ramphal, R.M. Strieter, L.L. Moldawer, P.A. Efron, Neutrophil mobilization from the bone marrow during polymicrobial sepsis is dependent on CXCL12 signaling, J. Immunol. 187 (2011) 911–918.
[5] M.B. Edmonson, E.L. Riedesel, G.P. Williams, G.P. Demuri, Generalized petechial rashes in children during a parvovirus B19 outbreak, Pediatrics 125 (2010) e787–e792.
[6] L. Chen, Mimotopes of cytolytic T lymphocytes in cancer immunotherapy, Curr. Opin. Immunol. 11 (1999) 219–222.
[7] B. Weigelin, M. Krause, P. Friedl, Cytotoxic T lymphocyte migration and effector function in the tumor microenvironment, Immunol. Lett. 138 (2011) 19–21.
[8] S. Sakaguchi, Regulatory T cells: key controllers of immunologic self-tolerance, Cell 101 (2000) 455–458.
[9] E.M. Shevach, Mechanisms of foxp3+ T regulatory cell-mediated suppression, Immunity 30 (2009) 636–645.
[10] Y. Takata, Y. Nakamoto, A. Nakada, T. Terashima, F. Arihara, M. Kitahara, K. Kakinoki, K. Arai, T. Yamashita, Y. Sakai, E. Mizukoshi, S. Kaneko, Frequency of CD45RO+ subset in CD4 + CD25(high) regulatory T cells associated with progression of hepatocellular carcinoma, Cancer Lett. 307 (2011) 165–173.
[11] C. Yee, S.R. Riddell, P.D. Greenberg, *In vivo* tracking of tumor-specific T cells, Curr. Opin. Immunol. 13 (2001) 141–146.
[12] G.A. Churchill, Fundamentals of experimental design for cDNA microarrays, Nat. Genet. 32 (Suppl.) (2002) 490–495.
[13] C.J. Stoeckert Jr., H.C. Causton, C.A. Ball, Microarray databases: standards and ontologies, Nat. Genet. 32 (Suppl.) (2002) 469–473.
[14] J.S. Reis-Filho, L. Pusztai, Gene expression profiling in breast cancer: classification, prognostication, and prediction, Lancet 378 (2011) 1812–1823.
[15] M. Honda, Y. Sakai, T. Yamashita, A. Sakai, E. Mizukoshi, Y. Nakamoto, I. Tatsumi, Y. Miyazaki, H. Tanno, S. Kaneko, Differential gene expression profiling in blood from patients with digestive system cancers, Biochem. Biophys. Res. Commun. 400 (2010) 7–15.
[16] Y. Sakai, M. Honda, H. Fujinaga, I. Tatsumi, E. Mizukoshi, Y. Nakamoto, S. Kaneko, Common transcriptional signature of tumor-infiltrating mononuclear inflammatory cells and peripheral blood mononuclear cells in hepatocellular carcinoma patients, Cancer Res. 68 (2008) 10267–10279.
[17] J. Wyckoff, W. Wang, E.Y. Lin, Y. Wang, F. Pixley, E.R. Stanley, T. Graf, J.W. Pollard, J. Segall, J. Condeelis, A paracrine loop between tumor cells and macrophages is required for tumor cell migration in mammary tumors, Cancer Res. 64 (2004) 7022–7029.
[18] H.H. van Ravenswaay Claasen, P.M. Kluin, G.J. Fleuren, Tumor infiltrating cells in human cancer. On the possible role of CD16+ macrophages in antitumor cytotoxicity, Lab. Invest. 67 (1992) 166–174.
[19] R.D. Leek, K.L. Talks, F. Pezzella, H. Turley, L. Campo, N.S. Brown, R. Bicknell, M. Taylor, K.C. Gatter, A.L. Harris, Relation of hypoxia-inducible factor-2 alpha (HIF-2 alpha) expression in tumor-infiltrative macrophages to tumor angiogenesis and the oxidative thymidine phosphorylase pathway in human breast cancer, Cancer Res. 62 (2002) 1326–1329.

[20] J.E. Talmadge, Immune cell infiltration of primary and metastatic lesions: mechanisms and clinical impact, Semin. Cancer Biol. 21 (2011) 131–138.

[21] H. Kobayashi, S. Dubois, N. Sato, H. Sabzevari, Y. Sakai, T.A. Waldmann, Y. Tagaya, Role of trans-cellular IL-15 presentation in the activation of NK cell-mediated killing, which leads to enhanced tumor immunosurveillance, Blood 105 (2005) 721–727.

[22] P. Allavena, A. Mantovani, Immunology in the clinic review series; focus on cancer: tumour-associated macrophages: undisputed stars of the inflammatory tumour microenvironment, Clin. Exp. Immunol. 167 (2012) 195–205.

[23] S.J. Cronin, J.M. Penninger, From T-cell activation signals to signaling control of anti-cancer immunity, Immunol. Rev. 220 (2007) 151–168.

[24] N.C. Twine, J.A. Stover, B. Marshall, G. Dukart, M. Hidalgo, W. Stadler, T. Logan, J. Dutcher, G. Hudes, A.J. Dorner, D.K. Slonim, W.L. Trepicchio, M.E. Burczynski, Disease-associated expression profiles in peripheral blood mononuclear cells from patients with advanced renal cell carcinoma, Cancer Res. 63 (2003) 6069–6075.

[25] J. Aaroe, T. Lindahl, V. Dumeaux, S. Saebo, D. Tobin, N. Hagen, P. Skaane, A. Lonneborg, P. Sharma, A.L. Borresen-Dale, Gene expression profiling of peripheral blood cells for early detection of breast cancer, Breast Cancer Res. 12 (2010) R7.

[26] M.J. Baine, S. Chakraborty, L.M. Smith, K. Mallya, A.R. Sasson, R.E. Brand, S.K. Batra, Transcriptional profiling of peripheral blood mononuclear cells in pancreatic cancer patients identifies novel genes with potential diagnostic utility, PLoS One 6 (2011) e17014.